



Melekhova, L., Schlaphorst, D., Blundy, J., Kendall, J. M., Connolly, C., McCarthy, A., & Arculus, R. (2019). Lateral Variation in Crustal Structure along the Lesser Antilles Arc from Petrology of Crustal Xenoliths and Seismic Receiver Functions. *Earth and Planetary Science Letters*, 516, 12-24. <https://doi.org/10.1016/j.epsl.2019.03.030>

Peer reviewed version

License (if available):
CC BY-NC-ND

Link to published version (if available):
[10.1016/j.epsl.2019.03.030](https://doi.org/10.1016/j.epsl.2019.03.030)

[Link to publication record in Explore Bristol Research](#)
PDF-document

This is the author accepted manuscript (AAM). The final published version (version of record) is available online via Elsevier at <https://www.sciencedirect.com/science/article/pii/S0012821X19301785> . Please refer to any applicable terms of use of the publisher.

University of Bristol - Explore Bristol Research

General rights

This document is made available in accordance with publisher policies. Please cite only the published version using the reference above. Full terms of use are available: <http://www.bristol.ac.uk/pure/user-guides/explore-bristol-research/ebr-terms/>

1 **Lateral Variation in Crustal Structure along the Lesser Antilles**
2 **Arc from Petrology of Crustal Xenoliths and Seismic Receiver**
3 **Functions**

4
5 Elena Melekhova^{1, *}, David Schlaphorst¹, Jon Blundy¹, J-Michael Kendall¹, Clare Connolly²,
6 Anders McCarthy¹, Richard Arculus²

7
8 ¹School of Earth Sciences, University of Bristol, Wills Memorial Building, Bristol BS8 1RJ,
9 UK.

10 ²RSES, Australian National University, Canberra, ACT 2601, Australia

11 * *Corresponding author, email address: lena.melekhova@bristol.ac.uk*

12
13 **Abstract**

14 We reconstruct crustal structure along the Lesser Antilles island arc using an inversion
15 approach combining constraints from petrology of magmatic crustal xenoliths and seismic
16 receiver functions. Xenoliths show considerable island-to-island variation in xenolith
17 petrology from plagioclase-free ultramafic lithologies to gabbros and gabbro-norites with
18 variable proportions of amphibole, indicative of changing magma differentiation depths.
19 Xenoliths represent predominantly cumulate compositions with equilibration depths in the
20 range 5 to 40 km. We use xenolith mineral modes and compositions to calculate seismic
21 velocities (v_P , v_S) and density at the estimated equilibration depths. We create a five-layer
22 model of crustal structure for testing against receiver functions (RF) from island seismic
23 stations along the arc. Lowermost layer (5) comprises peridotite with physical characteristics

24 of mantle xenoliths from Grenada. Uppermost layer (1) consists of 5 km of volcanoclastics
25 and sediments, whose physical properties are determined via a grid inversion routine. The
26 three middle layers (2) to (4) comprise igneous arc crust with compositions corresponding to
27 the xenoliths sampled at each island. By inversion we obtain a petrological best-fit for the RF
28 on each island to establish the nature and thicknesses of layers (2) to (4).

29

30 Along the arc we see variations in the depth and strength of both Moho and mid-crustal
31 discontinuity (MCD) on length-scales of tens of km. Moho depths vary from 25 to 37 km;
32 MCD from 11 and 32 km. The Moho is the dominant discontinuity beneath some islands (St.
33 Kitts, Guadeloupe, Martinique, Grenada), whereas the MCD dominates beneath others (Saba,
34 St. Eustatius). Along-arc variability in MCD depth and strength is consistent with variation in
35 estimated magmatic H₂O contents and differentiations depths that, in turn, influence xenolith
36 lithologies. A striking feature is steep, along-arc gradients in v_p similar to those observed at
37 other oceanic arcs. These gradients reflect abrupt changes in rates and processes of magma
38 generation in the underlying crust and mantle. We find no evidence for large, interconnected
39 bodies of partial melt beneath the Lesser Antilles. Instead, the crustal velocity structure is
40 consistent with magma differentiation in vertically-extensive, crystal mush-dominated
41 reservoirs. Along-arc variation in crustal structure may reflect heterogeneous upwelling
42 within the mantle wedge, itself driven by variation in slab-derived H₂O fluxes.

43

44 Highlights

- 45 • Arc crustal structure modelled by integrating petrology of 230 igneous xenoliths with
46 seismic data from 23 islands
- 47 • Crust comprises four layers defined on basis of xenolith composition, calculated
48 seismic properties and receiver functions

- 49 • Steep lateral velocity gradients and irregular along-arc variations in depth to Moho
50 and mid-crustal discontinuity
- 51 • Lateral variation consistent with island-to-island variation in xenolith petrology
- 52 • Velocity structure reflects heterogeneous upwelling within the mantle wedge, driven
53 by variation in slab-derived H₂O fluxes

54

55 **Keywords:** *island arc; crustal structure; magma differentiation; xenoliths; seismic properties*
56 *of rocks; receiver functions*

57

58

59 **1. Introduction**

60 *1.1 Background*

61 The layered nature of Earth's continental crust is the time-integrated product of magmatic
62 differentiation (Rudnick & Fountain, 1995). At convergent margin sites of active crust
63 formation, subducted slabs release H₂O-rich fluids into the mantle wedge, inducing partial
64 melting of peridotite to generate hydrous magmas of broadly basaltic composition.
65 Subsequent magmatic differentiation converts mantle-derived basalts into more evolved
66 compositions (e.g., andesites, granites) characteristic of mature continental crust. In the early
67 stages of differentiation Mg-rich mineral phases (olivine, pyroxenes) separate as ultramafic
68 cumulates from increasingly silica-rich melts. The appearance of plagioclase is delayed due
69 to the hydrous nature of the parent basalt, such that gabbroic (plagioclase-bearing) cumulates
70 only appear after ~40% crystallisation and andesitic melts with ~60 wt% SiO₂ after ~70%
71 crystallisation (Nandedkar et al., 2014). The exact proportions depend on the original
72 magmatic H₂O contents, differentiation depths and styles, and the extent of assimilation of
73 older crust. Regardless of these details, chemical differentiation at arcs generates significant

74 volumes of mafic and ultramafic solid residues. For bulk crustal compositions to become
75 broadly andesitic (Rudnick & Fountain, 1995) requires that some residual material is
76 displaced into the underlying mantle, either by downwards foundering ('delamination' – Jull
77 & Kelemen, 2001) or by upwards migration of the seismic Moho to coincide with the
78 appearance of plagioclase.

79

80 The constitution of the crust can be elucidated through studies of exhumed arc sections (e.g.,
81 Jagoutz & Behn, 2013), crustal xenoliths in volcanic rocks, or geophysical properties (e.g.,
82 Shillington et al., 2004; Kodaira et al., 2007). There is consensus that the continental crust
83 comprises at least three layers, characterised by downwards increasing P-wave velocities
84 (Rudnick & Fountain, 1995). Middle crust has an andesitic composition (61 wt% SiO₂; 3
85 wt% MgO), whereas lower crust is more mafic (52% SiO₂; 7% MgO). The uppermost crust is
86 predominantly felsic igneous (66% SiO₂, 2% MgO), although the prevalence of variously
87 fractured and unconsolidated volcanic and sedimentary rocks complicates the picture. For
88 this reason, it is reasonable to divide the upper layer into an igneous lower part and a
89 volcanic-sedimentary upper part. Some part of arc crust may comprise pre-existing,
90 overriding plate upon which the magmatic arc was built, although recent studies in western
91 Mognolia and the Izu Bonin Mariana arc (Gianola et al., 2017; Ishizuka et al., 2018) suggest
92 such material is conspicuously absent.

93

94 Globally, crustal thickness and velocity structure of oceanic arcs is highly variable (Fig. 1).
95 Some arcs conform to a simple three-layer structure (e.g., Sunda, Kermadec, New Britain),
96 whereas others are more complex (e.g., Mariana, Aleutians, New Ireland). The Moho is not
97 always well-resolved (e.g., Lesser and Greater Antilles). The apparent diversity of arc

98 structure, both between and within oceanic arcs, suggests significant complexity in crust
99 formation and evolution.

100

101 Resolving crustal structure is both a geophysical and petrological problem. Whereas
102 geophysics can resolve vertical and lateral variation in rock properties (v_P , v_S , density), their
103 interpretation in terms of igneous processes and lithologies requires a petrological
104 framework. To provide such a framework, we take as our study site the Lesser Antilles arc
105 (LAA), an active, slow-subduction intra-oceanic arc that is well instrumented geophysically,
106 well characterised geologically, and known to show significant along arc variation in
107 structure and petrology (Fig. 1, Boynton et al., 1979; Arculus & Wills, 1980). We combine
108 petrology and mineralogy of more than 200 crustal xenoliths from eleven volcanic islands
109 along LAA with seismic data from 23 remote island stations to investigate crustal structure in
110 such a way that one approach informs the other. We compare our findings to other oceanic
111 arcs and speculate on crustal structure and crust-forming processes more generally.

112

113 1.2 *The Lesser Antilles*

114 The LAA is an active, mature, intra-oceanic arc extending ~750 km from South America to
115 the Greater Antilles. The arc is a manifestation of slow, westward subduction of the North
116 and South American plates beneath the Caribbean plate. A review of the geological,
117 geochemical and tectonic setting of LAA is provided by Macdonald et al. (2002) and Smith
118 et al. (2013). LAA crustal structure was summarised by Schlaphorst et al. (2018).

119

120 LAA comprises eleven major volcanic islands and an archipelago of nineteen small islands
121 (the Grenadines) between St. Vincent and Grenada (Fig. 2). The arc bifurcates north of
122 Martinique producing inactive eastern and active western limbs. The active arc can be

123 divided into northern, central and southern segments with Wadati-Benioff zone dips varying
124 from 50-60° in the north to sub-vertical in the south. Over the last 0.1 Ma volcanism has been
125 more prominent in the central segment, as reflected in larger volcanic edifices. Average
126 magma production rates ($162 \text{ km}^3 \text{ km}^{-1} \text{ Myr}^{-1}$; Jicha & Jagoutz, 2015) fall at the lower end of
127 intra-oceanic arcs worldwide.

128

129 Compositions of LAA volcanic and plutonic rocks span the global arc array (Fig. 3), from
130 MgO-rich picrites and ankaramites on some islands (e.g., St. Vincent, Grenada, Martinique)
131 to voluminous dacites and rhyodacites on others (e.g., Dominica, St. Lucia). The northern and
132 central segments are predominantly andesitic with minor basalt, dacite and rare rhyolite (e.g.,
133 Toothill et al., 2006). The southern segment is dominated by basalts and basaltic-andesites,
134 including primitive, hydrous, MgO-rich (>12 wt%) basalts (e.g., Macdonald et al. 2002). The
135 high (>20 wt%) Al_2O_3 contents of basalts (Fig. 3b) reflect elevated magmatic H_2O contents.
136 On the basis of Fe-Mg partitioning between olivine and melt for magmas of known
137 $\text{Fe}_2\text{O}_3/\text{FeO}$, truly primitive magmas, i.e. those in equilibrium with olivine $\text{Fo}_{\geq 90}$, are limited
138 almost entirely to basalts ($\leq 50 \text{ wt SiO}_2$) from the southern segment (Fig. 3c). Very few more
139 evolved magmas, e.g. basaltic andesites ($\leq 55 \text{ wt SiO}_2$), may also be primitive. Isotopic data
140 show that the magmatic history of most LAA islands is dominated by igneous differentiation
141 processes with limited assimilation of older sialic crust or sediments (e.g., Macdonald et al.
142 2002; Toothill et al., 2006; Tollan et al., 2012; Bezard et al., 2014). Crustal contamination is
143 most pronounced on St. Lucia and Martinique (Bezard et al., 2015).

144

145 Igneous xenoliths occur on all LAA islands (Wills, 1974; Arculus & Wills, 1980). Xenoliths
146 are mineralogically and texturally diverse, both within individual islands and along the arc
147 (e.g., Arculus & Wills, 1980; Cooper et al., 2016; Camejo-Harry et al., 2018). Melekhova et

148 al. (2017) subdivide xenoliths into those that represent instantaneous solid extracts from one
149 or more magma batches (“cumulates”) and those whose compositions match erupted lavas
150 and have mineralogies and textures consistent with protracted solidification of magma
151 (“plutonics”). Cumulate xenoliths may contain significant quantities of trapped melt (e.g.
152 Stamper et al., 2014) and it is likely that there is a continuum from cumulate to plutonic types
153 according to this simple terminology. Geobarometry of LAA cumulate xenoliths (e.g.,
154 Stamper et al., 2014; Ziberna et al., 2017; Melekhova et al., 2017) yields crystallisation
155 pressures between 2 and 10 kbar, indicating that xenoliths sample igneous crust over a
156 significant depth range.

157

158 The LAA has been the subject of several major geophysical experiments (Boynton et al.,
159 1979; Christeson et al., 2008; Kopp et al., 2011; Laigle et al., 2013), summarised in Figure 1,
160 and a recent study of along-arc variations in crustal thickness using receiver functions
161 (Arnaiz-Rodríguez et al., 2016). Estimated crustal thickness ranges from 22 to 37 km.
162 Boynton et al. (1979) identified two seismic refractors that subdivide the crust into layers.
163 Their upper crustal layer is of plutonic igneous origin (Wadge, 1986) with an average v_P of
164 $6.2 \text{ km}\cdot\text{s}^{-1}$; its base varies significantly in depth (2 to 20 km) along strike. The uppermost
165 portion of the upper layer has lower seismic velocities ($v_P < 6 \text{ km}\cdot\text{s}^{-1}$) and densities and is
166 likely composed of volcanoclastic and sedimentary rocks with abundant fractures and pores
167 (Kiddle et al., 2010; Kopp et al., 2011). Gravity data from Guadeloupe (Gailler et al., 2013)
168 show that this layer is approximately 4 km thick. The lower crustal layer of Boynton et al.
169 (1979), immediately overlying the mantle, has average $v_P = 6.9 \text{ km}\cdot\text{s}^{-1}$ and is thought to
170 represent dense mafic igneous rocks, including cumulates.

171

172 Kopp et al. (2011) and Christeson et al. (2008) produced detailed seismic models of crustal
173 structure between Dominica and Guadeloupe and south of Grenada respectively. They
174 confirmed a layered crustal structure to that proposed by Boynton et al. (1979), albeit with
175 smoother vertical velocity gradient. For both profiles sub-arc v_p ranges from 1.4 to 7.3 km/s,
176 with most crust having v_p of 5.2 to 7.3 km/s (Fig. 1). Neither survey was able to constrain
177 well the sub-arc Moho.

178

179 **2. Crustal xenoliths**

180 During five field campaigns (2009-2017) we sampled every island in LAA, recovering just
181 under 900 coarse-grained igneous xenoliths both in situ and, predominantly, ex situ in river
182 drainages and reworked volcanic deposits. Xenoliths display great variation in mineralogy
183 and texture (Fig. 4) from hornblendite and wehrlite through gabbro and troctolite to quartz-
184 hornblende leuconorite and diorite (e.g., Wills, 1974; Arculus & Wills, 1980, Kiddle et al.,
185 2010, Stamper et al., 2014). The ubiquity of igneous xenoliths suggest that they represent
186 building blocks of LAA crust, providing a window into the entire differentiation history of
187 arc magmas from their source to eruption. Diversity in xenolith mineralogy reflects variation
188 in the composition of mantle-derived parent magmas, especially H₂O contents, and the
189 differentiation paths they follow through the crust (Melekhova et al., 2015).

190

191 *2.1 Xenolith assemblages and modes*

192 Despite their textural diversity, the mineralogy of crustal xenoliths is relatively
193 straightforward. More than 99% comprise permutations of eight mineral groups: olivine,
194 clinopyroxene, orthopyroxene, amphibole, plagioclase, magnetite, ilmenite and quartz.
195 Relative modal abundances of plagioclase and amphibole are significant (Fig. 5) and

196 plagioclase-free assemblages are uncommon, found only on Grenada, Bequia and St.
197 Vincent. Accessory minerals include apatite, analcime, biotite, sulphides and zircon.

198

199 Graphical comparison of xenolith mineral modes of from eleven islands is shown in Figure 5.

200 The overall mafic (plagioclase-poor) character of xenoliths from the southern islands of

201 Grenada, Carriacou and Bequia stands in sharp contrast to the predominance of felsic phases

202 (notably plagioclase) in St. Kitts, Montserrat, Guadeloupe and St. Lucia. Orthopyroxene is

203 rare or absent from southern islands xenoliths. The main mineral assemblages and textures,

204 from south to north, are as follows (cf. Arculus & Wills, 1980).

205 *Grenada* xenoliths are dominated by mafic minerals with abundant hornblende and

206 clinopyroxene and include plagioclase-free varieties (Fig. 4a) that are otherwise rare

207 (Stamper et al., 2014). Orthopyroxene is lacking; iddingsitised olivine is common. Most

208 xenoliths have adcumulate textures.

209 *Carriacou* xenoliths are dominated by clinopyroxene, amphibole and plagioclase. Olivine is

210 uncommon; orthopyroxene is lacking. A distinct feature is the presence of quartz and apatite

211 in diorites, the abundance of sulphides, and presence of interstitial analcime in few samples.

212 Textures range from adcumulates to porphyritic-phaneritic (Fig. 4b) and granoblastic

213 varieties.

214 *Bequia* xenoliths have the most diverse assemblages from a single island ranging from

215 ultramafic to felsic ($\leq 75\text{wt}\%$ plagioclase), with olivine (iddingsitized), amphibole,

216 clinopyroxene, plagioclase and spinel plus rare orthopyroxene and ilmenite. Textures range

217 from adcumulate to orthocumulate with variable crystallisation sequences (Camejo-Harry et

218 al., 2018).

219 *St. Vincent* xenoliths are characterised by abundant olivine and negligible orthopyroxene with

220 well-equilibrated, predominantly adcumulate textures and a lack of mineral zoning (Tollan et

221 al., 2012). Distinctive features include the presence of troctolites, with or without hornblende
222 (Fig. 4c), and olivine hornblendites.

223 *St. Lucia* xenoliths differ from other southern islands in being very evolved (high Fe/Mg) and
224 dominated by amphibole and plagioclase. Olivine is rare, orthopyroxene predominates over
225 clinopyroxene (Fig. 4d), and quartz and biotite are common. Cumulate textures are rare; most
226 samples resemble quenched mushes with abundant interstitial material.

227 *Martinique* xenoliths are predominantly igneous, with sparse cordierite-bearing hornfelsed.
228 All xenoliths are plagioclase-bearing, with variable proportions of olivine (troctolites),
229 clinopyroxene, orthopyroxene, amphibole and spinel, commonly with interstitial melt
230 (Cooper et al., 2016).

231 *Dominica* xenoliths show low variability assemblages dominated by olivine, clinopyroxene
232 and plagioclase (Fig. 4e), often with well-equilibrated textures (Zibera et al., 2017) that
233 resemble those on Carriacou. Olivine is partially iddingsitized.

234 *Guadeloupe* xenoliths are dominated modally by plagioclase. Relatively primitive samples
235 contain varying proportions of olivine, pyroxene, amphibole, and spinel, whereas more
236 evolved samples contain quartz, biotite, magnetite, ilmenite, apatite, orthoclase, sulfide and
237 rare zircon (Fig. 4f). Most xenoliths appear isotropic and homogeneous, yet texturally
238 diverse, with both igneous and metamorphic (hornfelsed) varieties.

239 *Montserrat* xenoliths, similar to Guadeloupe and *St. Lucia*, are distinctively felsic and
240 olivine-free. Assemblages are dominated by noritic and gabbroic anorthosites and
241 hornblende-gabbros. Other common varieties include quartz-diorite and metamorphosed
242 biotite-gabbro. Cumulate and crescumulate textures abound (Kiddle et al., 2010).

243 *St. Kitts* xenoliths are dominated by exceptionally calcic plagioclase ($An_{\leq 100}$; Melekhova et
244 al., 2017) and amphibole, typically in reaction relationship with pyroxene and olivine. Both
245 cumulate and plutonic varieties occur. Important characteristics include the presence of two

246 pyroxenes, biotite, apatite, and coexisting ilmenite and magnetite. Interstitial melt is
247 common.

248 *St. Eustatius* mineral assemblages and textures are similar to those of Martinique (Cooper et
249 al., submitted). Orthopyroxene occurs only in non-cumulate (plutonic) gabbros.

250

251 **3. Methods**

252 *3.1 Petrological constraints: physical properties of crustal xenoliths*

253 Fifty to seventy xenoliths per island were studied and divided into textural and mineralogical
254 groups from which representative samples were analysed. Mineral major element chemistry
255 was analysed on polished carbon-coated thin-sections using Cameca SX100 and JEOL 8530F
256 electron microprobes at University of Bristol and the Australian National University
257 respectively. Analytical conditions were 15 or 20 kV accelerating voltage and 10 nA focused
258 beam. Modal abundances of major mineral phases (≥ 0.5 vol%) were obtained by point-
259 counting (900 to 3000 points per thin-section). Volume modes were converted into mass
260 fraction modes using appropriate mineral densities.

261

262 Physical properties of rocks (v_p , v_s , density) can be calculated from mineral compositions
263 and proportions, provided that a reasonable estimate of temperature and pressure are
264 available (e.g., Müntener and Ulmer, 2006, Jagoutz and Behn, 2013). We retrieved physical
265 properties of LAA xenoliths, using their mass fraction modes and mineral compositions, with
266 the algorithm of Hacker & Abers (2016) for the nine major islands with seismic stations:
267 Grenada (Stamper et al., 2014); St. Vincent (Tollan et al., 2012); St. Lucia (Wills, 1974 and
268 our unpublished data); Martinique (Cooper et al., 2016); Dominica (Wills, 1974);
269 Guadeloupe (our unpublished data); Montserrat (Kiddle et al., 2010); St. Kitts (Melekhova et
270 al., 2017); and St. Eustatius (Cooper et al., submitted). Modal abundances for each island are

271 reported in Supplementary Table S2. For all solid solutions we calculated the proportions of
272 end-members; for amphibole we used the generic “hornblende” in the Hacker & Abers
273 (2016) database. The modal proportion of quartz is consistently very low, making distinction
274 between α -quartz and β -quartz (cf. Jagoutz & Behn, 2013) immaterial for calculating
275 physical properties

276

277 Pressure-temperature (P–T) conditions of xenolith equilibration were estimated using a
278 variety of geobarometers and geothermometers (e.g., Ziberna et al., 2017; Supplementary
279 Tab. S2), together with constraints from phase equilibrium experiments performed on
280 appropriate starting compositions (cf. Stamper et al., 2014). For the majority of islands
281 studied magmatic H₂O contents were estimated based on melt inclusion analyses (Bouvier et
282 al., 2008, Melekhova et al., 2017, Cooper et al., submitted). Knowing H₂O content, phase
283 assemblages and mineral composition of studied xenoliths (particularly, Fo content of olivine
284 and An content of plagioclase) helped us to narrow the existing experimental dataset (~1500
285 experiments) to obtain reliable P and T. The full dataset of calculated physical properties and
286 P-T estimates, including methods used and uncertainties, is given in Supplementary Table S2.
287 Because of the counteracting effects of increasing P and T on physical properties, realistic
288 deviations from estimated P-T values have little bearing on the calculated properties, i.e. <1%
289 relative in v_P and <0.008 in v_P / v_S ratio. We also calculated physical properties of peridotite
290 beneath LAA using mantle xenoliths from Grenada (Parkinson et al., 2003; Stamper et al.,
291 2014). Mantle xenoliths are not found on any other island in the LAA.

292

293 *3.1 Geophysical constraints: seismic properties and structure*

294 Broadband seismic data from various regional networks were collected (Fig. 2); for
295 Montserrat, Guadeloupe and Martinique more than one station is available. Teleseismic

296 events were filtered using a 2nd order Butterworth bandpass filter from 0.4 Hz to 3 Hz and
297 only events with a clear P-phase were selected (Schlaphorst et al., 2018). We use the
298 extended-time multi-taper frequency-domain cross-correlation receiver-function (ETMTRF)
299 of Helffrich (2006) and an H–K stacking method similar to Thompson et al. (2010). H–K
300 stacking is based on theoretical arrival times of converted phases and derives values for the
301 depth (H) to a seismic discontinuity and the average P-wave to S-wave ratio ($K=v_p/v_s$) of the
302 overlying crustal layer. As noted by Schlaphorst et al. (2018), a significant disadvantage of
303 H–K stacking is its reliance on a single discontinuity separating two layers, such as upper and
304 lower crust (mid-crustal discontinuity - MCD) or crust and mantle (Moho). In the case of
305 layered crust with multiple discontinuities peaks in the RF caused by different discontinuities
306 can overlie each other, complicating the H–K stacking results. For example, on Martinique,
307 H–K stacking shows a strong, well-resolved discontinuity at 28.3 ± 1.1 km (Fig. 3a), whereas
308 on St. Lucia, the discontinuity is placed much deeper (46.5 ± 1.8 km) and the solution is very
309 poorly resolved. At some islands H values are too shallow, producing unrealistic depths to
310 the Moho or missing it altogether. Schlaphorst et al. (2018) concluded that H–K stacking
311 results for layered crust can be easily misinterpreted and proposed an inversion modelling
312 approach to overcome this problem. In combination with petrology, their approach provides a
313 powerful tool to distinguish between one or more MCD and the Moho, and to resolve the
314 seismic properties (v_p , v_p/v_s) of multiple layers, even at island seismic stations with relatively
315 high noise.

316

317 We apply a combination of the grid-search and inversion methods of Schlaphorst et al. (2018)
318 to the RF assuming a four-layer crust plus underlying mantle within the following
319 petrological framework: uppermost crustal layer (1) composed of loosely consolidated and

320 fractured volcanoclastic rocks, sediments and lavas; upper (2), middle (3) and lower (4)
321 crustal layers composed of plutonic igneous rocks; and a peridotitic mantle layer (5).

322

323 Physical properties of surface layer (1) are controlled primarily by fracture density and
324 degree of consolidation, rather than the lithology *per se*. Therefore, for layer (1), we first
325 invert the RF using the method of Ammon et al. (1990) assuming five 1-km thick subsidiary
326 layers (1a-e). Total thickness of layer (1) is fixed at 5 km, consistent with the geophysical
327 data of Christeson et al. (2008), Kiddle et al. (2010) and Gailler et al. (2013).

328

329 Crustal layers (2), (3) and (4) consist of the various xenolith lithologies for which physical
330 properties were calculated. Beneath each island we identify a range of plausible lithologies
331 for each of the three layers, based on our P-T estimates (Fig. 6c, Supplementary Tab. S2). On
332 the basis of our textural observations and thermobarometric calculations layer (4) is found to
333 be consistently cumulate in character, whereas layers (2) and (3) represent mixtures of
334 cumulate and plutonic (solidified magmas or mushes) lithologies (Supplementary Tab. S2).
335 We then perform a grid-search using the calculated v_p , v_s , v_p/v_s and density of each lithology
336 to find those that yields a best-fit to the RF for that island. We assume that all melt has either
337 been extracted or is isolated at very low melt fraction along grain boundaries, consistent with
338 the low melt fractions observed in xenoliths (see below).

339

340 Physical properties of mantle layer (5) were based on Grenadian peridotite xenoliths
341 (Parkinson et al., 2003; Stamper et al., 2014): $v_p=8.00 \text{ km}\cdot\text{s}^{-1}$, $v_s=4.43 \text{ km}\cdot\text{s}^{-1}$, $\rho=3.33$
342 $\text{kg}\cdot\text{m}^{-3}$. The same values were used for the entire LAA as there is insufficient evidence from
343 petrology or seismology to justify along-arc variation in mantle v_p . For comparison the

344 seismic profiles of Christeson et al (2008) and Kopp et al. (2011) yield sub-arc mantle v_P of
345 7.7 km/s and 8.0 km/s, respectively.

346

347 **4. Results**

348 Our physical property calculations indicate that the permissible range of v_P/v_S for each island
349 is narrow (Fig. 6a, Supplementary Tab. S2). On average, v_P/v_S varies between 1.79 to 1.88
350 for v_P from 6.2 to 7.4 km·s⁻¹ (Fig. 6 a & b and Supplementary Tab. S2). In contrast to
351 Müntener & Ulmer (2006) calculated xenolith v_P values never exceed 7.8 km·s⁻¹ and are
352 therefore consistently lower than the mantle (Fig. 6a). The relationship between density and
353 v_P is non-linear (Fig. 6b). Densities of mantle xenoliths from Grenada and ultramafic crustal
354 xenoliths from Grenada and St Vincent are similar, ~ 3.3 g/cm³, however the majority of
355 LAA crustal xenoliths has a narrow range of densities, 2.8-3.0 g/cm³. Lithologies dominated
356 by amphibole + plagioclase \pm quartz result in v_P values down to 6.2 km·s⁻¹, with relatively
357 low v_P/v_S (Fig. 6a), whereas calculated v_P/v_S for plagioclase-dominated lithologies ($\geq 80\%$)
358 are up to 1.91 at comparable v_P (Fig. 6a).

359

360 Depth distribution of LAA xenoliths (Fig. 6c) suggests that v_P of the igneous crust is
361 variable: 6.2 to 7.0 km·s⁻¹ in layer (2), 6.4 to 7.2 km·s⁻¹ in layer (3) and 6.8 to 7.4 km·s⁻¹ in
362 layer (4). The range of xenolith physical properties (v_P , v_S , v_P/v_S , density) and depth ranges
363 define the petrological parameter space of our grid-search method to find the combination of
364 lithology and thickness for each crustal layer beneath each island that best fits the
365 corresponding RF. Despite our extensive sampling, on the islands of St. Lucia and St.
366 Eustatius, we have no xenolithic record of potential lower crustal lithologies. Initial models
367 for these two islands were therefore run without layer (4). However, a good fit to RF was not
368 achieved, so we introduced a plausible lower crust layer (4) taking values from neighbouring

369 St. Vincent and St. Kitts respectively. On any island (e.g. Montserrat) where the best-fit
370 thickness of a given layer lay within error of zero this layer was omitted, reducing to a three-
371 layer crustal structure. Our inversion approach considers only new, magmatic arc crust.
372 Schlaphorst et al. (2018) demonstrated that incorporating a layer of vestigial proto-Caribbean
373 crust (pCc) into the crustal model does not change the depth of the discontinuities in the
374 inversion results unless the pCc is unrealistically thick (≥ 20 km).

375

376 Representative best-fit model velocity profiles and synthetic RF for two islands (Martinique
377 and Grenada) are illustrated in Figure 7. For Martinique two strong discontinuities at 27 km
378 (Moho) and 13 km (MCD1) were identified (Fig.7a). A weak additional discontinuity
379 (MCD2) lies just above the Moho at 24 km depth. The best fit for Martinique was achieved
380 with the following lithologies: layer (2) troctolite, (3) olivine gabbro and (4) hornblende
381 gabbro. For Grenada, the Moho is identified at 29 km and both MCDs are strong (12
382 and 14 km) with a small intervening low velocity zone (Figs.7b and 8). The best fit for
383 Grenada was achieved with following lithologies: layer (2) poikilitic-hornblende gabbro, (3)
384 hornblende gabbro and (4) clinopyroxene hornblendite. Modelled velocity profiles and RF
385 for all studied islands, obtained as for Martinique and Grenada, are provided in
386 Supplementary Material and summarised in terms of crustal lithologies in Table 1.

387

388 **5. Crustal structure of the Lesser Antilles arc**

389 The v_p , v_s , v_p/v_s and density constraints from xenolith petrology combined with RF inversion
390 provide new insights into LAA velocity structure (Figs. 8). MCD depths and v_p for layers (2)
391 to (4) are in an excellent agreement with previous work on the southern segment of the arc
392 (Fig.1 and Schlaphorst et al., 2018). The Moho was not directly observed seismically in
393 previous studies but was estimated to lie between 24 and 35 km depth (e.g., Boynton et al.

394 1979; Christeson et al., 2008; Kopp et al., 2011; Laigle et al., 2013; Arnaiz-Rodríguez et al.,
395 2016).

396

397 Our obtained crustal structure (Fig. 8) shows that MCD and Moho depths are highly variable
398 over surprisingly short, along-arc distances of tens of kilometres. Arnaiz-Rodríguez et al.
399 (2016) arrived at a similar conclusion, with up to 10 km change in Moho depth across
400 Guadeloupe alone. Our Moho depths vary from 24 km (St. Eustatius) to 38 km (e.g. St. Kitts
401 and Dominica). The seismic velocity of layers (2), (3) and (4) also varies laterally. The
402 modelled four-layer crustal structure yields two MCD, however one of them is usually
403 stronger than the other. Depth to the MCD between layers (3) and (4) changes from 12 to 32
404 km, whilst that between layers (2) and (3) is from 6 to 15 km. Beneath St. Lucia, layer (2) is
405 very thin (~2 km); beneath Montserrat it is absent. Beneath Grenada 2 km-thick layer (3) has
406 a lower v_P than overlying layer (2); St. Eustatius has a very thin (1 km) layer (4) with lower
407 v_P than overlying layer (3). Variation in v_P along the arc is non-systematic. For example, we
408 observe a high v_P mid-crustal layer (3) under Martinique and St. Eustatius (6.97 and 7.14
409 km/s respectively), but a low layer (3) v_P of 6.55 km/s under Grenada (Figs. 8 and 9). Lower
410 crustal layer (4) v_P varies from 7.43 km/s beneath Montserrat to 6.75 km/s beneath St. Kitts
411 just 90 km to the north. Our along-arc variability in discontinuity depths (Fig. 8) is similar to
412 that of Boynton et al. (1979).

413

414 Our preferred final, five-layer P-wave velocity model (Fig. 8) for LAA is as follows. The 5
415 km-thick upper layer (1) has highly variable v_P due to lithological heterogeneity. P-wave
416 velocities are 6.2 to 6.86 $\text{km}\cdot\text{s}^{-1}$ in the upper crust (layer 2) in the depth range of 6 to 15 km,
417 6.46 to 7.18 $\text{km}\cdot\text{s}^{-1}$ in the middle crust (layer 3) in the depth range 12 to 32 km, and 6.75 to
418 7.43 $\text{km}\cdot\text{s}^{-1}$ in the lower crust (layer 4) in the depth range 26 to 38 km.

419

420 **5. Interpretation and discussion**

421 Our petrologically-informed crustal model for LAA (Fig. 8) resembles that of other oceanic
422 island arcs (Fig. 1) including those, subject to high-resolution seismic experiments, such as
423 the northern segment of Izu-Bonin (Kodaira et al. 2007) and the Aleutians (Shillington et al
424 2004). To facilitate comparison of LAA with these two arcs, in Figure 9 we present seismic
425 velocity profiles for all three arcs using the same vertical and horizontal scales and consistent
426 v_p contour intervals of $<6 \text{ km}\cdot\text{s}^{-1}$, $6.0\text{-}6.8 \text{ km}\cdot\text{s}^{-1}$, $6.8\text{-}7.8 \text{ km}\cdot\text{s}^{-1}$ and $>7.8 \text{ km}\cdot\text{s}^{-1}$.

427

428 Several key features emerge. Like LAA, the northern segment of Izu-Bonin and the Aleutians
429 show the expected downwards increase in v_p , together with abrupt lateral variations on
430 wavelengths of a few tens of km, as previously noted by Kodaira et al. (2007). Both the 6.8
431 km s^{-1} and 7.8 km s^{-1} contours show considerable along-arc variation in depth, by up to 20
432 km. Beneath some volcanic islands (e.g., Dominica and Montserrat in LAA; South Sumisu
433 and Nii-jima in Izu-Bonin; Unalaska and Chuginadak in Aleutians) material with v_p in the
434 range $6.8\text{-}7.8 \text{ km}\cdot\text{s}^{-1}$ extends to very shallow crustal depths, in some cases impinging almost
435 directly on crustal layer (1). In all three arcs there is no clear correlation between the depths
436 to the 6.8 and 7.8 km s^{-1} contours, suggestive of strong decoupling between thicknesses of the
437 different crustal layers. Despite the greater spatial resolution of the crustal structure in Izu-
438 Bonin and Aleutians arcs (Fig. 9), it would appear that the crust in all three arcs displays the
439 same abrupt lateral variations in physical properties. The diversity of crustal lithologies, as
440 recorded by xenoliths, is responsible for the change of seismic properties along the LAA
441 (Figs. 5, 6 and 8). Lateral variations in v_p in Izu-Bonin and Aleutians may have a similar
442 lithological cause, although there is not the same xenolith record with which to evaluate this
443 possibility.

444

445 Tamura et al. (2016) compared crustal thickness along the Izu-Bonin arc, obtained from
446 seismology, with bathymetry. They found a correlation between water depth and crustal
447 thickness, suggesting that water depth can be used to estimate crustal thickness under the arc.
448 They ascribe this variation to changes in the nature of mantle-derived magmas, from basalt to
449 andesite, along the arc. We constructed the along-arc profile for LAA using bathymetric data
450 for the eastern Caribbean (Fig. 8). Although there is some correlation, it is not as uniform and
451 straightforward as shown for Izu-Bonin by Tamura et al. (2016), perhaps reflecting the lower
452 spatial resolution of our study. Nonetheless, water depth and crustal thickness link well for
453 the southern segment of the arc and for Dominica and Guadeloupe, the largest islands with
454 the greatest crustal thickness. The most obvious misfit is Martinique, where, despite the
455 island's considerable size, the crust is relatively thin.

456

457 Geochemical data from LAA (Fig. 3c) do not support a wide variety of mantle-derived
458 magmas along the arc, in contrast to the proposition of Tamura et al. (2016) for Izu-Bonin.
459 The relationship between our calculated crustal structure and magmatic history (magma
460 compositions, fluxes, volatile contents etc) of each island in LAA remains to be investigated.
461 However, we can speculate as to possible explanations for along-arc lithological changes.

462

463 Variations in v_P could arise through variations in trapped melt fraction within rocks of
464 broadly similar seismic velocities. The presence of partial melt reduces both v_P and v_S , but
465 increases v_P/v_S significantly, due to the stronger reduction of v_S . The extent of v_P/v_S reduction
466 depends not only on melt fraction, but also on its distribution. In regions with significant,
467 distributed partial melt v_P/v_S ratios of up to 2.00 are observed (Hammond et al., 2011).
468 However, LAA islands whose H–K stacking results agree with those from RF inversion (e.g.

469 Montserrat, Martinique) indicate v_P/v_S significantly less than 2, suggesting rather little
470 interconnected partial melt. In their H–K stacking study of the LAA Arnaiz-Rodrigues et al.
471 (2016) also found v_P/v_S consistently in the range 1.77-1.87. Melt-rich regions of reduced v_P
472 would correspond to increased v_P/v_S in Figure 8. If melts are fully interconnected, i.e. melt
473 wets grain boundaries completely, then it is possible to calculate their effect on v_P and v_P/v_S .
474 Using the experimental data of Chantel et al. (2016) for anhydrous basaltic melt in an olivine
475 matrix, we calculate that 5 vol% of fully interconnected melt will reduce v_P from 7.6 to 6.6
476 km s^{-1} with a corresponding increase in v_P/v_S from 1.79 to 2.01. There is no evidence for
477 $v_P/v_S > 1.9$ in either the Aleutians (Shillington et al., 2013) or LAA (Arnaiz-Rodrigues et al,
478 2016), ruling out variability in interconnected melt fraction as the principal cause of lateral v_P
479 gradients. Nonetheless, it is likely, given the active nature of these arcs, that some isolated
480 pockets of higher melt fraction exist, beyond the resolution of the seismic methods used.
481 Alternatively, it may be that the wetting properties of hydrous andesite and basaltic andesite
482 melts lead to less melt connectivity and consequently less extreme increase in v_P/v_S than
483 obtained by Chantel et al. (2016).

484

485 Normal faults orthogonal to the arc (e.g., Feuillet et al., 2002) could also lead to abrupt lateral
486 variations in crustal structure. However, the apparent decoupling of upper, mid and lower
487 crustal layer thicknesses mitigates against such an explanation. Variations in thickness of the
488 pre-subduction crust on the over-riding plate may also play a role, but, as noted above, this is
489 hard to evaluate from the seismic data alone. It seems more likely that normal faults, where
490 present, act to accommodate lateral thickness (and density) variations, for example through
491 isostatic readjustment, rather than create them. Evidence for relative vertical movements
492 along the LAA comes from observation of drowned coral reefs. For example, at Les Saintes,
493 Guadeloupe, Leclerc et al. (2014), estimate subsidence rates of 0.4 mm/yr over the past 125

494 kyr. Leclerc et al. (2015) derive a similar subsidence rate (0.3 mm/yr) for drowned reefs off
495 the coast of Martinique. This subsidence is ascribed to arc-parallel extension (Feuillet et al.,
496 2002), but could conceivably be driven instead by vertical block movement in response to
497 lateral variation in crustal thickness and/or density. In ductile crust vertical motion driven by
498 lateral density gradients has been proposed as a mechanism for generating crustal
499 stratification (e.g. Glazner, 1994) and may ultimately lead to sinking of dense, lower crustal
500 cumulates into the mantle, i.e. delamination (Jagoutz & Behn, 2013). However, the positive
501 (albeit non-linear) correlation of v_P and density (Fig. 6b; Supplementary Table S2) does not
502 support a convective process, unless it is enhanced by a significant fraction of partial melt
503 serving to reduce the density of higher v_P cumulates. We argue above that such melt, if
504 present, cannot be significant in volume and/or interconnected.

505

506 Our preferred interpretation of LAA crustal structure is along-arc variation in the
507 mechanisms of melt generation and differentiation. These variations can arise from
508 instabilities along the mantle-slab interface, such as those predicted by the numerical models
509 of Gerya et al. (2006), or by generation of hot, buoyant regions within the mantle wedge, as
510 demonstrated by Tamura et al. (2002) for northern Japan. Tamura et al. (2002) suggest that
511 low velocity regions in the crust are linked to “hot fingers” in the underlying mantle. It is not
512 clear whether the generation of “hot fingers” is due to lateral variations in wedge temperature
513 or in the proportion of partial melt generated by the influx of slab-derived fluids, or a
514 combination of both. In Gerya et al.’s (2006) numerical models upwellings, or “cold plumes”,
515 arising from the slab interface generate lateral variations in melt productivity and
516 composition within the mantle wedge. The finger-like protuberances of high- and low- v_P
517 crustal material observed in Figure 8 could correspond to the influence of cold plumes as they
518 impinge on the over-riding plate or to the rise of hot fingers. Both features afford a

519 mechanism for arc-parallel, convective motion in the mantle wedge that could drive along-arc
520 variability in magma flux and chemistry. Along-arc flow of the asthenosphere has been
521 proposed as an explanation of trench-parallel seismic anisotropy beneath the Tonga-
522 Kermadec and the Marianas arcs (e.g., Menke et al., 2015; Smith et al., 2001). However, the
523 pattern of anisotropy in the upper-mantle wedge tends to be highly variable, suggesting
524 variations in the style of upper-mantle flow from one subduction zone to another.

525

526 Generation of buoyant anomalies in the mantle wedge may, in part, be controlled by the
527 amount of water liberated from the slab (e.g., by serpentine dehydration) that can change
528 mantle density both by metasomatism (e.g. formation of amphibole or phlogopite peridotite)
529 and partial melting. This explanation is consistent with the observations of Schlaphorst et al.
530 (2016), based on b-value variations in upper plate seismicity along LAA, and on variations in
531 the ratio of fluid mobile and immobile trace elements in magmas along the Aleutians (Manea
532 et al., 2014). Seismic anomalies related to heterogeneous upwelling in the mantle wedge
533 beneath the Izu-Bonin arc have been observed by Obana et al. (2010), who also implicate
534 them in lateral variations in both crustal structure and magma chemistry.

535

536 Lateral variations in the magma differentiation mechanisms along the arc also play a role. It
537 is now recognised that many crustal magmatic systems comprise vertically extensive
538 magmatic mushes (Cashman et al. 2017), wherein differentiation occurs not by simple crystal
539 settling from a dominantly liquid magma chamber, but by upwards, reactive flow of buoyant,
540 low-degree melts through a crystal-rich (mush) framework. The products of such reactions, in
541 terms of solid residues, are modulated by the composition (especially H₂O content) and flux
542 of the basaltic, mantle-derived magmas feeding the base of the crust and the internal
543 architecture of the mush itself (Solano et al. 2012). Variations in input magma chemistry and

544 flux could be driven by the heterogeneous upwelling phenomena described above. Different
545 magma compositions and intensities of upwelling along the arc would drive different types of
546 mush reservoirs and, consequently, solid residue lithologies. The igneous xenolith record for
547 LAA is consistent with a laterally variable, mushy system, variously infiltrated and modified
548 by melts (Tollan et al. 2012; Stamper et al. 2014; Cooper et al. 2016; Melekhova et al. 2017,
549 Camejo-Harry et al. 2018), as demonstrated by variations in modal mineralogy along the arc
550 (Fig. 5). Melt infiltration drives reactions that produce diverse eruptible melts and variously
551 amphibole-bearing and amphibole-free plutonic rocks with differing physical properties (Fig.
552 6). The migration of v_p contours up and down the crustal column would then reflect the
553 changing mineralogy of the solid residues as partial melts migrate and react upwards.

554

555 In general, solid residues (xenoliths) become more magnesian (higher v_p) with depth (Fig. 5)
556 consistent with polybaric differentiation of mantle-derived magmas (Melekhova et al. 2015).
557 It is unclear whether the 7.8 km s^{-1} contour in Fig. 9 marks the crustal-mantle boundary (i.e.
558 Moho *sensu strictu*), or the change from mafic to ultramafic cumulates. As noted above and
559 by Müntener & Ulmer (2006), mantle peridotite and ultramafic cumulates have strikingly
560 similar physical properties that are not readily resolved by the seismic methods employed
561 here. The difficulty of recognising the Moho in the LAA, and in arcs more generally, likely
562 reflects the preponderance of ultramafic cumulates at depth, as proposed for the fossil
563 Kohistan arc by Jagoutz & Behn (2013).

564

565 **6. Conclusions**

566 We have elucidated crustal structure along strike in the LAA using a novel approach that
567 integrates xenolith petrology and seismology. Our approach affords several advantages over a
568 purely seismological approach, especially in arc settings at stations with significant noise,

569 where the H–K stacking method is prone to ambiguity. Combining several local networks, it
570 has been possible to generate a detailed picture of crustal structure beneath the major islands
571 of LAA. We show that arc crust is highly variable along-arc on relatively short wavelengths.
572 One explanation for such variability in the delivery of water to the arc, plausibly via
573 heterogeneous mantle upwellings that in turn affect the temperature and composition of the
574 mantle-derived melts supplied to the base of the crust (e.g., Parman et al 2011) and the solid
575 residues produced during differentiation (e.g., Melekhova et al., 2015). We tentatively note a
576 spatial correlation between changes in crustal v_p and subducting transform faults (Fig. 2), that
577 are likely water-rich and serpentinised, as previously suggested by Schlaphorst et al. (2016).
578 In relatively low productivity arcs, such as LAA, crust appears to be composed
579 predominantly of the solid residues of differentiation processes, with little interstitial trapped
580 melt. This process is distinct from a classical model of crustal differentiation in which solids
581 progressively separate from large volumes of melt in crustal magma chambers. Thus, the
582 mush-dominated architecture that appears to dominate many crustal magmatic systems
583 (Cashman et al., 2017) may also control the structure of the arc crust. Using magmatic
584 xenoliths to reconstruct crustal velocity structure is clearly a fruitful avenue that is
585 complimentary to seismic experiments and to the reconstruction of seismic velocities from
586 exhumed arc sections.

587

588 Data Access Statement: All underlying data are provided in full within this paper, either in
589 the main text or as accompanying supplementary material.

590

591 **Acknowledgements**

592 This work was supported by NERC grants NE/N001966/1, NE/K004883/1, NE/K014978/1
593 and NE/K010824/1 and ERC Advanced Grant CRITMAG (Blundy). We thank S. Sparks and

594 members of the NERC-funded VoiLA research consortium (NE/K010824/1) for useful
 595 discussions, C. Hawkesworth for insightful comments and suggestions for the manuscript, T.
 596 Nichols for providing some of the xenolith modes from St. Lucia, and Y. Tamura and O.
 597 Jagoutz for reviews of the manuscript.

598

599

600 References

601 Ammon, C., Randall, G., Zandt, G., 1990. On the Non-uniqueness of Receiver Function Inversion. *Geophysical*
 602 *Journal International* 95, 15303–15318. doi:10.1029/JB095iB10p15303.

603

604 Arculus, R.J., Wills, K.J., 1980. The petrology of plutonic blocks and inclusions from the Lesser Antilles island
 605 arc. *Journal of Petrology* 21, 743–799.

606

607 Arnaiz-Rodríguez, M.S., Schmitz, M., Audemard, F., 2016. La estructura cortical del arco de las Antillas
 608 Menores estimada a partir de la técnica de funciones receptoras. *Revista mexicana de ciencias geológicas* 33,
 609 286–296.

610

611 Bezar, R., Davidson, J.P., Turner, S., Macpherson, C.G., Lindsay, J.M., Boyce, A.J., 2014. Assimilation of
 612 sediments embedded in the oceanic arc crust: myth or reality? *Earth and Planetary Science Letters* 395, 51–60.
 613 doi.org:10.1016/j.epsl.2014.03.038

614

615 Bezar, R., Turner, S., Davidson, J.P., Macpherson, C.G. and Lindsay, J.M., 2015. Seeing through the effects of
 616 crustal assimilation to assess the source composition beneath the southern Lesser Antilles Arc. *Journal of*
 617 *petrology*, 56, 815–844. doi: 10.1093/petrology/egv018

618

619 Bouvier, A. S., Metrich, N. & Deloule, E., 2008. Slab-derived fluids in the magma sources of St. Vincent
 620 (Lesser Antilles arc): volatile and light element imprints. *Journal of Petrology* 49,1427–1448.
 621 doi.org:10.1093/petrology/egn031

622

623 Boynton, C., Westbrook, G., Bott, M., Long, R., 1979. A seismic refraction investigation of crustal structure
 624 beneath the Lesser Antilles arc. *Geophysical Journal of the Royal Astronomical Society* 58, 371–393.

625

626 Camejo-Harry, M., Melekhova, E., Blundy, J., Attridge, W., Robertson, R. and Christopher, T., 2018. Magma
 627 evolution beneath Bequia, Lesser Antilles, deduced from petrology of lavas and plutonic xenoliths.
 628 *Contributions to Mineralogy and Petrology*, 173, 77, doi.org:10.1007/s00410-018-1504-z

629

630 Cashman, K.V., Sparks, R.S.J., Blundy, J.D., 2017. Vertically extensive and unstable magmatic systems: A
 631 unified view of igneous processes. *Science* 355, eaag3055. doi:10.1126/science.aag3055.

632

633 Chantel, J., Manthilake, G., Andrault, D., Novella, D., Yu, T., Wang, Y., 2016. Experimental evidence supports
 634 mantle partial melting in the asthenosphere. *Science advances* 2, e1600246. doi:10.1126/sciadv.1600246.

635

636 Christeson, G., Mann, P., Escalona, A., Aitken, T., 2008. Crustal structure of the Caribbean-northeastern South
 637 America arc-continent collision zone. *Journal of Geophysical Research–Solid Earth* 113.
 638 doi:10.1029/2007JB005373.

639

640 Cooper, G.F., Davidson, J.P., Blundy, J.D., 2016. Plutonic xenoliths from Martinique, Lesser Antilles: evidence
 641 for open system processes and reactive melt flow in island arc crust. *Contributions to Mineralogy and Petrology*
 642 171, 87. doi:10.1007/s00410-016-1299-8.

643

- 644 Feuillet, N., Manighetti, I., Tapponnier, P., Jacques, E., 2002. Arc parallel extension and localization of volcanic
645 complexes in Guadeloupe, Lesser Antilles. *Journal of Geophysical Research Solid Earth* 107, B12.
646 doi: 10.1029/2001JB000308.
647
- 648 Gailler, L.S., Martelet, G., Thion, I., Bouchot, V., Lebrun, J.F., Münch, P., 2013. Crustal structure of
649 Guadeloupe islands and the Lesser Antilles arc from a new gravity and magnetic synthesis. *Bulletin de la*
650 *Société Géologique de France* 184, 77–97. doi:10.2113/gssgfbull.184.1-2.77.
651
- 652 Gerya, T.V., Connolly, J.A., Yuen, D.A., Gorczyk, W., Capel, A.M., 2006. Seismic implications of mantle
653 wedge plumes. *Physics of the Earth and Planetary Interiors* 156, 59–74. doi:10.1016/j.pepi.2006.02.005.
654
- 655 Gianola, O., Schmidt, M.W., Jagoutz, O., Sambuu, O., 2017. Incipient boninitic arc crust built on denudated
656 mantle: the Khantaishir ophiolite (western Mongolia). *Contributions to Mineralogy and Petrology* 172, 92.
657 doi:10.1007/s00410-017-1415-4.
658
- 659 Glazner, A.F., 1994. Foundering of mafic plutons and density stratification of continental crust. *Geology*, 22,
660 435-438. doi.org:10.1130/0091-7613(1994)022<0435:FOMPAD>2.3.CO;2
661
- 662 Hacker, B.R., Abers, G.A., 2004. Subduction factory 3: An excel worksheet and macro for calculating the
663 densities, seismic wave speeds, and H₂O contents of minerals and rocks at pressure and temperature.
664 *Geochemistry, Geophysics, Geosystems* 5. doi:10.1029/2003GC000614.
665
- 666 Hammond, J., Kendall, J.M., GW, S., Keir, D., Ebinger, C., Ayele, A., Belachew, M., 2011. The nature of the
667 crust beneath the Afar triple junction: Evidence from receiver functions. *Geochemistry Geophysics Geosystems*
668 12. doi:10.1029/2011GC003738.
669
- 670 Helffrich, G., 2006. Extended-time multitaper frequency domain cross-correlation receiver-function estimation.
671 *Bulletin of the Seismological Society of America* 96, 344–347. doi.org:10.1785/0120050098
672
- 673 Ishizuka, O., Hickey-Vargas, R., Arculus, R.J., Yogodzinski, G.M., Savov, I.P., Kusano, Y., McCarthy, A.,
674 Brandl, P.A. and Sudo, M., 2018. Age of Izu–Bonin–Mariana arc basement. *Earth and Planetary Science*
675 *Letters*, 481, pp.80-90. doi.org:10.1016/j.epsl.2017.10.023
676
- 677 Jagoutz, O., Behn, M.D., 2013. Foundering of lower island-arc crust as an explanation for the origin of the
678 continental Moho. *Nature*, 504, 131-134
679
- 680 Jicha, B.R., Jagoutz, O., 2015. Magma production rates for intraoceanic arcs. *Elements* 11, 105–111.
681 doi:10.2113/gselements.11.2.105.
682
- 683 Jull, M., Kelemen, P.B., 2001. On the conditions for lower crustal convective instability. *Journal of Geophysical*
684 *Research: Solid Earth* 106, 6423–6446. doi:10.1029/2000JB900357.
685
- 686 Kiddle, E., Edwards, B., Loughlin, S., Petterson, M., Sparks, R., Voight, B., 2010. Crustal structure beneath
687 Montserrat, Lesser Antilles, constrained by xenoliths, seismic velocity structure and petrology. *Geophysical*
688 *Research Letters* 37. doi:10.1029/2009GL042145.
689
- 690 Kodaira, S., Sato, T., Takahashi, N., Tamura, Y., Tatsumi, Y., Kaneda, Y., 2007. Seismological evidence for
691 variable growth of crust along the Izu intraoceanic arc. *Journal of Geophysical Research–Solid Earth* 112.
692 doi.org/10.1029/2006JB004593.
693
- 694 Kopp, H., Weinzierl, W., Becel, A., Charvis, P., Evain, M., Flueh, E., Gailler, A., Galve, A., Hirn, A.,
695 Kandilarov, A., Klaeschen, D., Laigle, M., Papenberg, C., Planert, L., Roux, E., Team, T., Team, T., 2011. Deep
696 structure of the central Lesser Antilles Island Arc: Relevance for the formation of continental crust. *Earth and*
697 *Planetary Science Letters* 304, 121–134. doi:10.1016/j.epsl.2011.01.024.
698
- 699 Laigle, M., Hirn, A., Sapin, M., Bécel, A., Charvis, P., Flueh, E., Diaz, J., Lebrun, J.F., Gesret, A., Raffaele, R.
700 and Galvé, A., 2013. Seismic structure and activity of the north-central Lesser Antilles subduction zone from an
701 integrated approach: Similarities with the Tohoku forearc. *Tectonophysics*, 603, pp.1-20.
702 doi:10.1016/j.tecto.2013.05.043
703

- 704 Leclerc, F., Feuillet, N., Cabioch, G., Deplus, C., Lebrun, J.F., BATHYSAINTES cruise scientific party, Bazin,
705 S., Beauducel, F., Boudon, G., LeFriant, A., De Min, L., Melezan, D., 2014. The Holocene drowned reef of Les
706 Saintes plateau as witness of a long-term tectonic subsidence along the Lesser Antilles volcanic arc in
707 Guadeloupe. *Marine Geology*, 355, 115-135. doi.org:10.1016/j.margeo.2014.05.017
708
- 709 Leclerc, F., Feuillet, N., Perret, M., Cabioch, G., Bazin, S., Lebrun, J.-F., Saurel, J.M., 2015. The reef platform
710 of Martinique: Interplay between eustasy, tectonic subsidence and volcanism since Late Pleistocene. *Marine
711 Geology*, 369, 34-51. doi.org:10.1016/j.margeo.2015.08.001
712
- 713 Macdonald, R., Hawkesworth, C. J. & Heath, E., 2000. The Lesser Antilles volcanic chain: a study in arc
714 magmatism. *Earth-Science Reviews* 49, 1-76. doi.org:10.1016/S0012-8252(99)00069-0.
715
- 716 Manea, V.C., Leeman, W.P., Gerya, T., Manea, M. and Zhu, G., 2014. Subduction of fracture zones controls
717 mantle melting and geochemical signature above slabs. *Nature communications* 5, 5095. doi:
718 10.1038/ncomms6095
719
- 720 Melekhova, E., Blundy, J., Robertson, R., Humphreys, M.C., 2015. Experimental evidence for polybaric
721 differentiation of primitive arc basalt beneath St. Vincent, Lesser Antilles. *Journal of Petrology* 56, 161-192.
722 doi.org:10.1093/petrology/egu074
723
- 724 Melekhova, E., Blundy, J., Martin, R., Arculus, R., Pichavant, M., 2017. Petrological and experimental evidence
725 for differentiation of water-rich magmas beneath St. Kitts, Lesser Antilles. *Contributions to Mineralogy and
726 Petrology* 172, 98. doi.org:10.1007/s00410-017-1416-3
727
- 728 Menke, W., Y. Zha, S. C., Webb, D. K., Blackman., 2015. Seismic anisotropy indicates ridge-parallel
729 asthenospheric flow beneath the Eastern Lau Spreading Center, *J. Geophys. Res. Solid Earth.*, 120, pg. 976-
730 992, doi:10.1002/2014JB011154
731
- 732 Müntener, O., Ulmer, P., 2006. Experimentally derived high-pressure cumulates from hydrous arc magmas and
733 consequences for the seismic velocity structure of lower arc crust. *Geophysical Research Letters* 33.
734 doi:10.1029/2006GL027629.
735
- 736 Nandedkar, R.H., Ulmer, P., Müntener, O., 2014. Fractional crystallization of primitive, hydrous arc magmas:
737 an experimental study at 0.7 GPa. *Contributions to Mineralogy and Petrology* 167, 1015. doi:10.1007/
738 s00410-014-1015-5. doi: 10.1007/s00410-014-1015-5
739
- 740 Obana, K., Kamiya, S., Kodaira, S., Suetsugu, D., Takahashi, N., Takahashi, T., Tamura, Y., 2010. Along-arc
741 variation in seismic velocity structure related to variable growth of arc crust in northern Izu-Bonin intraoceanic
742 arc. *Geochemistry, Geophysics, Geosystems* 11. doi:10.1029/2010GC003146. q08012.
743
- 744 Parkinson, I. J., Arculus, R. J. & Eggins, S. M., 2003. Peridotite xenolith from Grenada, Lesser Antilles Island
745 Arc. *Contribution to Mineralogy and Petrology* 146, 241-262
746
- 747 Rudnick, R.L., Fountain, D.M., 1995. Nature and composition of the continental crust: a lower crustal
748 perspective. *Reviews of geophysics* 33, 267-309. doi:10.1029/95RG01302.
749
- 750 Schlaphorst, D., Kendall, J., Collier, J., Verdon, J., Blundy, J., Baptie, B., Latchman, J., Massin, F., Bouin, M.,
751 2016. Water, oceanic fracture zones and the lubrication of subducting plate boundaries – insights from
752 seismicity. *Geophysical Journal International* 204, 1405-1420. doi:10.1093/gji/ggv509.
753
- 754 Schlaphorst, D., Melekhova, E., Kendall, J.-M., Blundy, J., Latchman, J.L., 2018. Probing layered arc crust in
755 the Lesser Antilles using receiver functions. *R. Soc. open sci.* 5:180764. doi.org:10.1098/rsos.180764
756
- 757 Shillington, D.J., Van Avendonk, H.J., Holbrook, W.S., Kelemen, P.B., Hornbach, M.J., 2004. Composition and
758 structure of the central Aleutian island arc from arc-parallel wide-angle seismic data. *Geochemistry,
759 Geophysics, Geosystems* 5. doi:10.1029/2004GC000715.
760
- 761 Shillington, D.J., Van Avendonk, H.J.A., Behn, M.D., Kelemen, P.B., Jagoutz, O., 2013. Constraints on the
762 composition of the Aleutian arc lower crust from VP/VS. *Geophysical Research Letters*, 40, 2579-84.
763 doi.org:10.1002/grl.50375

- 764
765 Smith, G. P., Wiens, D.A. Fischer, M., Dorman, L., Webb., S., Hildebrand, J. (2001). A complex pattern of
766 mantle flow in the Lau Backarc, *Science*, 292, 713–716. doi:10.1126/science.1058763
767
768 Smith, A.L., Roobol, M.J., Mattioli, G.S., Fryxell, J.E., Daly, G., Fernandez, L.A., 2013. The Volcanic Geology
769 of the Mid-Arc Island of Dominica. Volume 496. Geological Society of America.
770
771 Solano, J., Jackson, M., Sparks, R., Blundy, J., Annen, C., 2012. Melt segregation in deep crustal hot zones: a
772 mechanism for chemical differentiation, crustal assimilation and the formation of evolved magmas. *Journal of*
773 *Petrology* 53, 1999–2026. doi:10.1093/petrology/egs041.
774
775 Stamper C.C., Blundy, J., Arculus, R.J., Melekhova, E., 2014. Petrology of plutonic xenoliths and volcanic
776 rocks from Grenada, Lesser Antilles. *Journal of Petrology* 55, 1353-1387, doi:10.1093/petrology/egu027
777
778 Tamura, Y., Tatsumi, Y., Zhao, D., Kido, Y., Shukuno, H., 2002 Hot fingers in the mantle wedge: new insights
779 into magma genesis in subduction zones. *Earth and Planetary Science Letters*, 197, 105-116.
780 doi.org:10.1016/S0012-821X(02)00465-X.
- 781 Tamura, Y., Sato T., Fujiwara, T., Kodaira, S., Nichols A., 2016. Advent of continents: A new hypothesis.
782 *Scientific Report* 6, 33517. doi:10.1038/srep33517.
- 783 Thompson, D., Bastow, I., Helffrich, G., Kendall, J.M., Wookey, J., Snyder, D., Eaton, D., 2010. Precambrian
784 crustal evolution: Seismic constraints from the Canadian Shield. *Earth and Planetary Science Letters* 297, 655–
785 666. doi.org/10.1016/j.epsl.2010.07.021
- 786 Tollan, P., Bindeman, I., Blundy, J., 2012. Cumulate xenoliths from St. Vincent, Lesser Antilles island arc: a
787 window into upper crustal differentiation of mantle-derived basalts. *Contributions to Mineralogy and Petrology*
788 163, 189–208. doi:10.1007/s00410-011-0665-9.
789
790 Toothill, J., Williams, C., Macdonald, R., Turner, S., Rogers, N., Hawkesworth, C., Jerram, D., Ottley, C.,
791 Tindle, A., 2006. A complex petrogenesis for an arc magmatic suite, St Kitts, Lesser Antilles. *Journal of*
792 *Petrology* 48, 3–42. doi:10.1093/petrology/egl052.
793
794 Wadge, G., 1986. The dykes and structural setting of the volcanic front in the Lesser Antilles island arc. *Bulletin*
795 *of Volcanology* 48, 349–372. doi:10.1007/BF01074466.
796
797 Wills, K. J. A., 1974. The geological history of Southern Dominica and plutonic nodules from the Lesser
798 Antilles. Unpublished Ph.D. Thesis, University of Durham, England.
799
800 Ziberna, L., Green, E.C., Blundy, J.D., 2017. Multiple-reaction geobarometry for olivine-bearing igneous rocks.
801 *American Mineralogist* 102, 2349–2366. doi:10.2138/am-2017-6154.
802

803

804 **Figure Captions**

805 **Figure 1.** Comparison of crustal structure of a selection of intra-oceanic arcs based on
806 seismic refraction experiments (updated and modified from Boynton et al., 1979). The range
807 in v_P (km/s) within individual crustal layers is shown by the double-ended arrows; asterisks
808 denote an average value for multiple layers. Seismic discontinuities are shown by solid
809 horizontal lines; the Moho is indicated by an additional dotted line. A question mark indicates

810 a poorly resolved Moho. Fine dashed lines represent changes in v_P without associated
 811 discontinuity. References for the arcs are provided by Boynton et al. (1979) with the
 812 following additions: Lesser Antilles – (a: S of Grenada, Christeson et al. 2008; b: S of
 813 Guadeloupe, Kopp et al. 2011); Japan – (a: Honshu, Iwasaki et al. 2001); (b: Hokkaido,
 814 Iwasaki et al. 2004); Sunda – (Kieckhefer et al. 1980); Aleutians – (Shillington et al. 2004);
 815 Izu – (Kodaira et al. 2007); Mariana – (Takahashi et al. 2007).

816

817 **Figure 2.** Map of the Lesser Antilles arc showing the seismic broadband stations used in this
 818 study (red triangles) and newly deployed stations (in yellow) by VoiLA (a NERC-funded
 819 multidisciplinary consortium project). The western, active branch of the arc is shown in
 820 black, the eastern, inactive branch in grey. There are 12 seismic stations on Montserrat in
 821 close proximity. Approximate extrapolation of fracture zones from the downgoing plate to
 822 the sub-arc is illustrated by dotted black lines: FT – Fifteen-Twenty; Ma – Marathon; Me –
 823 Mercurius; Ve – Vema; Do – Doldrums (Schlaphorst et al. 2016).

824

825 **Figure 3.** Bulk-rock MgO (a) and Al₂O₃ (b) variations in Lesser Antilles lavas plotted against
 826 SiO₂. (c) Plot of SiO₂ against of FeO^T/MgO ratio. Data with measured FeO and Fe₂O₃ are
 827 marked by circles with a black outline on (a) and (b). Pink solid line on (c) corresponds to an
 828 FeO/MgO ratio that would correspond to equilibrium with olivine Fo₉₀, using $Kd^{ol-liq}=0.3$.
 829 Magmas that lie on or below this line are potentially primary, i.e. in equilibrium with mantle
 830 olivine Fo_{≥90}. Potential primary magmas in LAA are predominantly basalts. Note absence of
 831 high-MgO basalts in northern islands and abundance of high-Al₂O₃ basalts and basaltic
 832 andesites. Data are from GEOROC.

833

834 **Figure 4.** Photomicrographs of representative xenolith textures and compositions in plane-
 835 polarised (ppl) and cross-polarised light (xpl). **(a)** Clinopyroxenite (sample GR5-1) with
 836 adcumulate texture (ppl) from Grenada showing large, unzoned clinopyroxene and
 837 hornblende with minor iddingsitised olivine. **(b)** Clinopyroxene-gabbro (CR6) from
 838 Carriacou (xpl) with porphyritic-phaneritic texture showing clinopyroxene grains with partial
 839 reaction to amphibole, and abundant oxides. **(c)** Hornblende-bearing troctolite (xpl) with
 840 adcumulate texture (VS8) from St Vincent. **(d)** Hornblende gabbro (SL63) with
 841 mesocumulate texture from St. Lucia (SL63). **(e)** Olivine-hornblende gabbro (ppl) with
 842 adcumulate texture from Dominica (DC102), showing considerable alteration of olivine to
 843 iddingsite. **(f)** Granodiorite (xpl) from Guadeloupe (GD40) showing equigranular texture.
 844 Mineral abbreviations: cpx (clinopyroxene), opx (orthopyroxene), pl (plagioclase), ox (Fe-Ti
 845 oxides), id (iddingsite), qz (quartz).

846

847 **Figure 5.** Modal proportion of minerals by mass in crustal xenoliths along LAA, ordered
 848 from North to South. Xenoliths for individual islands are listed from bottom to top in order of
 849 decreasing Fo content of olivine, followed by Mg# of clinopyroxene, followed by An content
 850 of plagioclase. Data from Wills, 1974; Tollan et al., 2012; Stamper et al 2014; Cooper et al.,
 851 2016; Melekhova et al 2017; Camejo-Harry et al., 2018; unpublished - Supplementary Table
 852 S1. Notice more mafic nature and almost complete absence of orthopyroxene in xenoliths
 853 from the southern segment compared to central and northern segments. Arrows and letters
 854 denote samples shown on Figure 4.

855

856 **Figure 6.** Seismic properties of LAA xenoliths calculated using the algorithm of Hacker &
 857 Abers (2016). All xenoliths are crustal igneous rocks, except for mantle xenoliths marked
 858 with a cross. Phase proportions were obtained by point counting (Fig. 5); P-T conditions of

859 equilibration were estimated by thermobarometry and/or phase petrology. **(a)** v_P/v_S ratio
 860 versus v_P . Note fields of plagioclase-rich ($\geq 80\%$ plagioclase) xenoliths with relatively low v_P
 861 and high v_P/v_S (dashed grey line) and amphibole-rich ($\geq 80\%$ amphibole + plagioclase \pm
 862 quartz) xenoliths (dashed purple line). **(b)** v_P versus density (ρ). Hornblende and
 863 clinopyroxene-rich compositions from Grenada, St Vincent and one from Montserrat show
 864 significantly higher velocities and densities compared to other xenolith lithologies. The
 865 lowest density and velocity xenoliths are granodiorites from Guadeloupe. **(c)** Relative depths,
 866 estimated from thermobarometry and phase petrology, versus v_P . Different layers evaluated
 867 by RF inversion are shown: UC – upper-crustal layer (2), MC – mid-crustal layer (3), LU –
 868 low-crustal layer (4) and M – mantle layer (5).

869

870 **Figure 7.** Modeled 1-D profiles for density, v_P and v_S (top) and Receiver Functions (bottom)
 871 for Martinique (A) and Grenada (B). Lower panels show the stacked RFs (black) and the
 872 model RFs (red); grey lines show the pointwise 2σ -jackknife uncertainties. Modelling results
 873 for all other islands can be found in Supplementary Material.

874

875 **Figure 8.** Compilation of inversion results along LAA from south (Grenada) to north (St. Vincent).
 876 Along-arc bathymetry in the top panel was constructed using latitude-longitude-elevation
 877 data from the global multi-resolution topography (GMRT) synthesis via GeoMapApp, and
 878 the multi-point “path profiler” tool in GlobalMapper20. The bottom panel shows the crustal
 879 v_P structure beneath each island based on a five-layer inversion (four crustal layers plus
 880 mantle) using RFs and petrological constraints as described in the text. v_P values (km/s) of
 881 each layer are shown for clarity. The Moho is denoted by a thick black line. Note
 882 heterogeneity of the uppermost layer (1) and the abrupt lateral variations in v_P and crustal
 883 layer thicknesses. Note that only two crustal layers could be resolved beneath Montserrat.

884

885

886 **Figure 9.** Comparison of v_p structure beneath three oceanic arcs: (a) Northern segment of
887 Izu-Bonin (Kodaira et al, 2007); (b) Aleutians (Shillington et al. 2004); and (c) Lesser
888 Antilles (this study). Contour intervals of 6.0, 6.8 and 7.8 km s⁻¹ are chosen to aid
889 comparison. All figures drafted to the same vertical and horizontal scale. Lesser Antilles
890 structure (c) adapted from Fig 8 using the method in Supplementary Information with
891 velocities between islands estimated using a third-order polynomial interpolation. Volcanic
892 islands denoted with triangles, using the following abbreviations: (a) Os – Oh-shima; Nij –
893 Nii-jima; Myk – Miyake-jima; Mkr – Mikura-jima; Krs – Kurose; Hcj – Hachijo-jima; Shc –
894 South Hachijo; Ags – Aoga-shima; Myn – Myojin; Sms – South Sumisu; Ssc – South
895 Sumisu; Tsm – Torishima; (b) Seg – Seguam; Am – Amukta; Yun – Yunaska; Her – Herbert;
896 Chu – Chuginadak; (c) Ski – St. Kitts; Seus – St. Eustatius (Statia). Note low velocity mid-
897 crustal layer under Grenada and Grenadines, and high velocity region under Statia. Izu-Bonin
898 and Aleutians seismic data were obtained at much higher resolution than for LAA, yet the
899 overall lateral variations in v_p structure and crustal thickness are similar in all three arcs.

Figure 1
[Click here to download Figure: Figure 1.pdf](#)

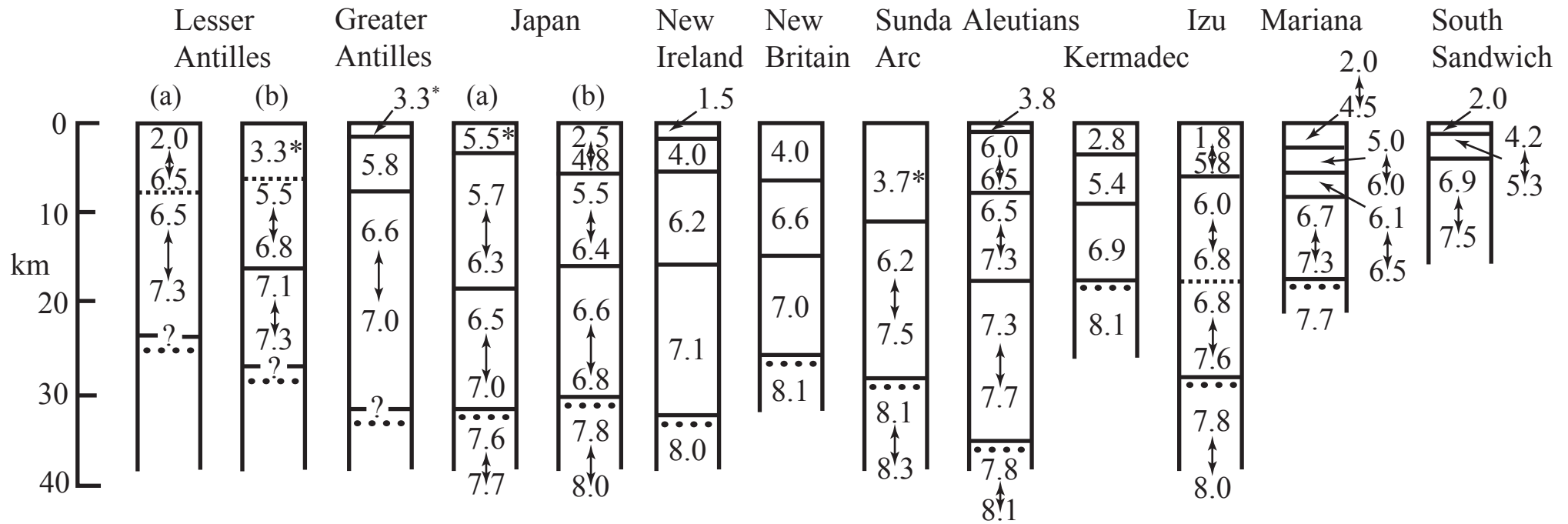


Figure 2
[Click here to download Figure: Figure 2.pdf](#)

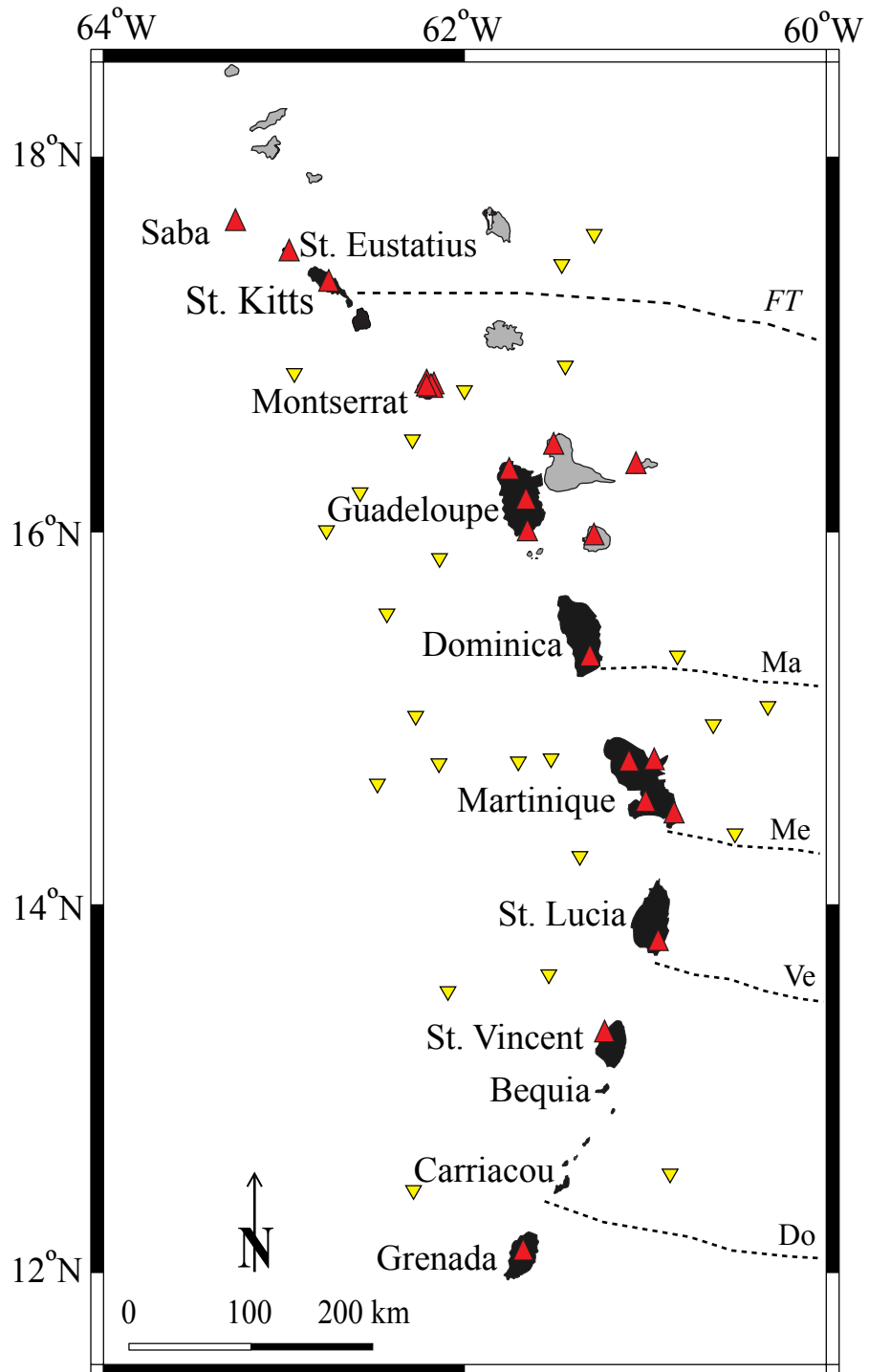


Figure 3
[Click here to download Figure: Figure 3.pdf](#)

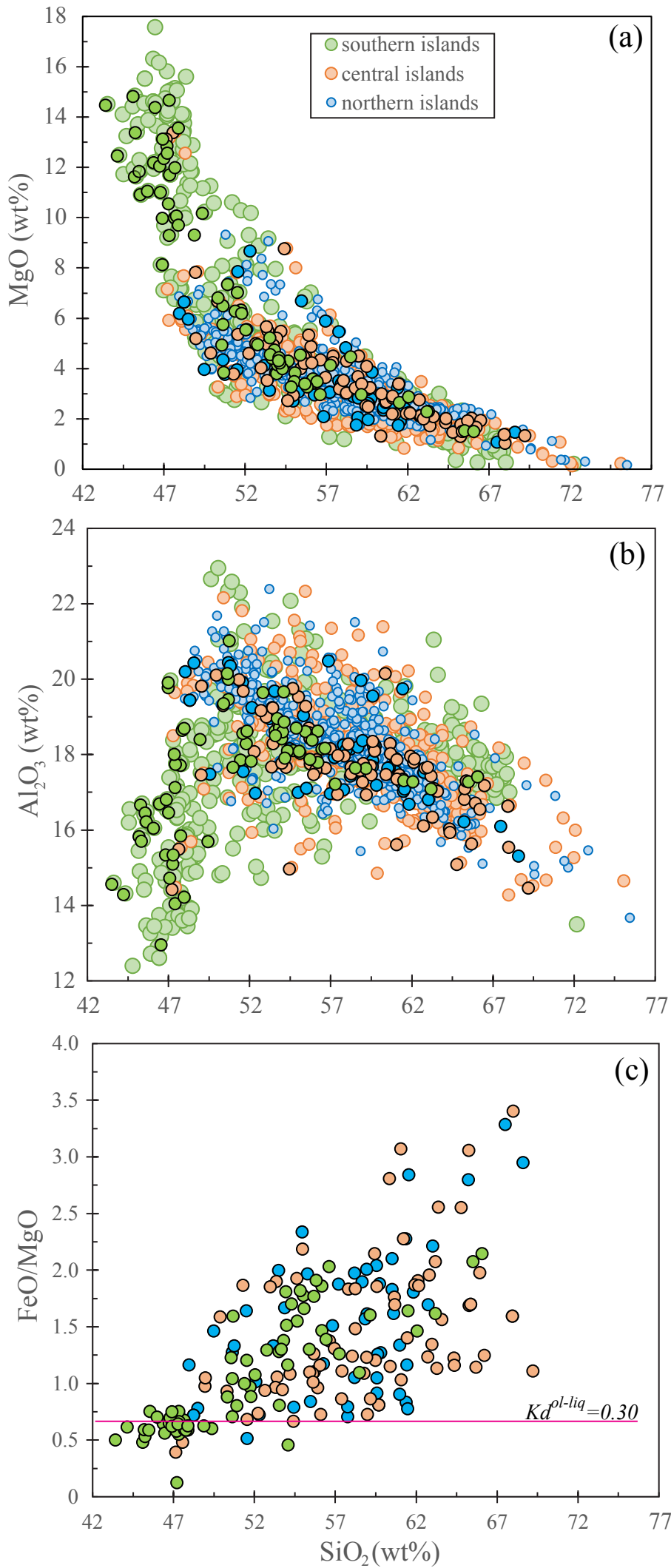


Figure 4
Click here to download Figure: Figure 4.pdf

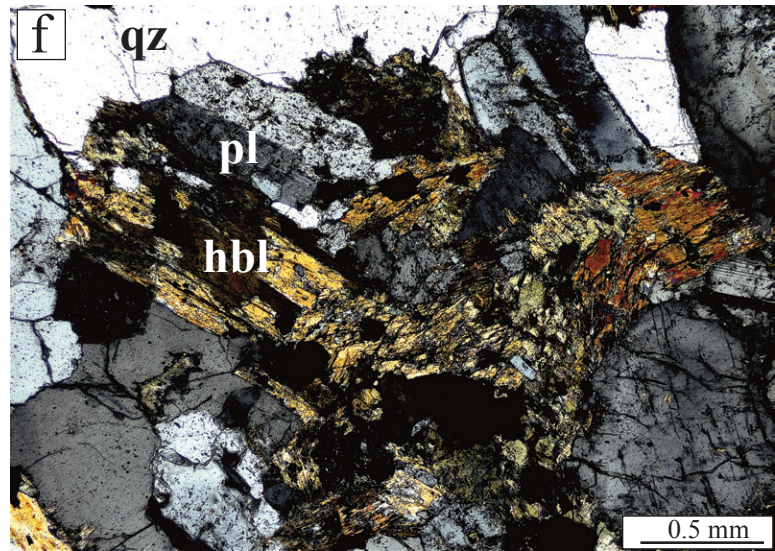
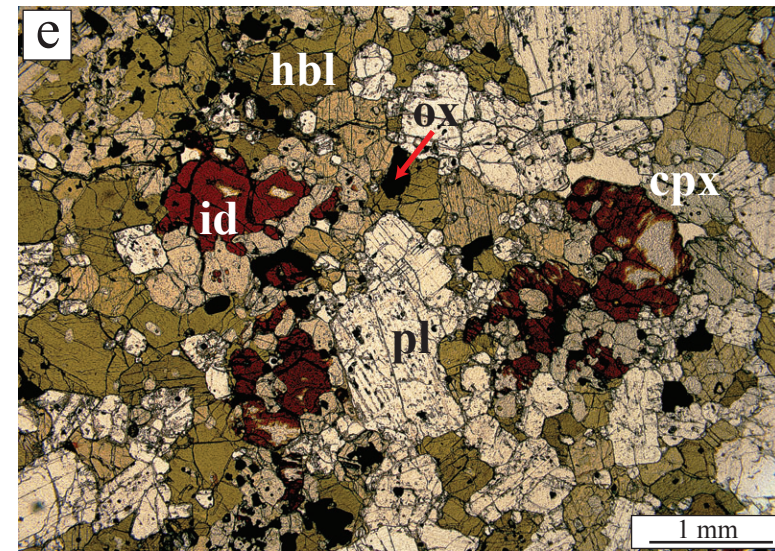
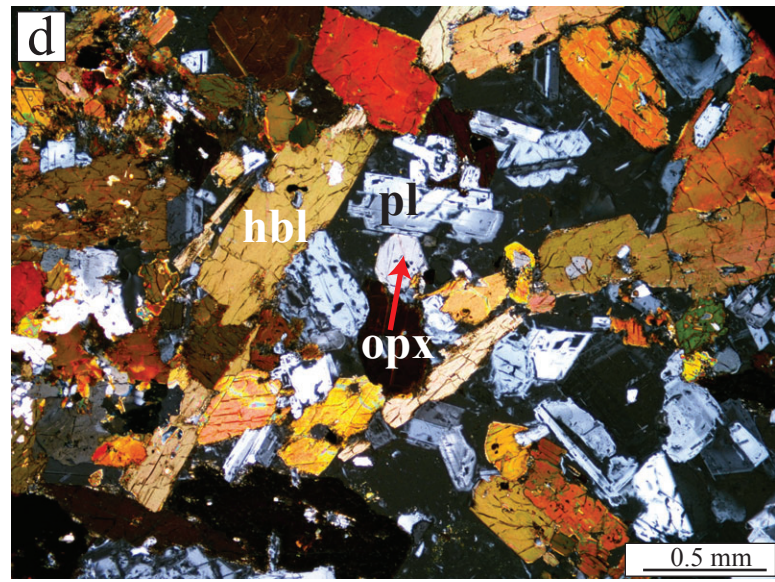
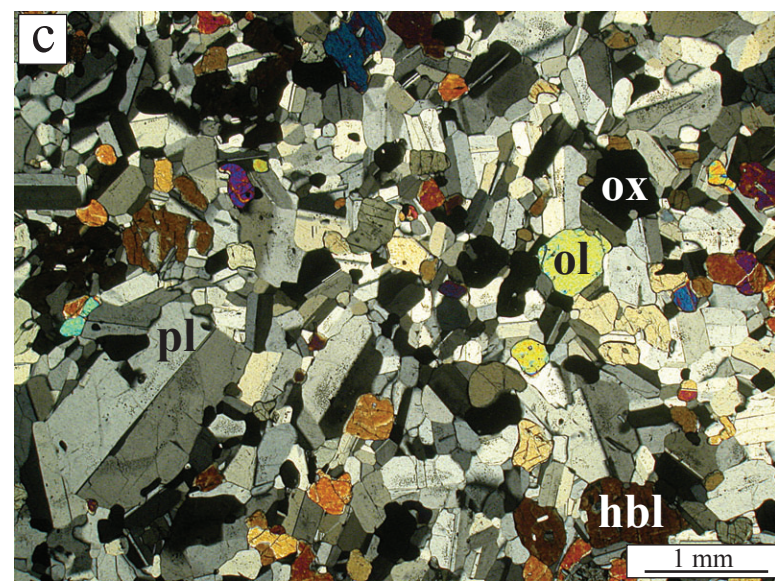
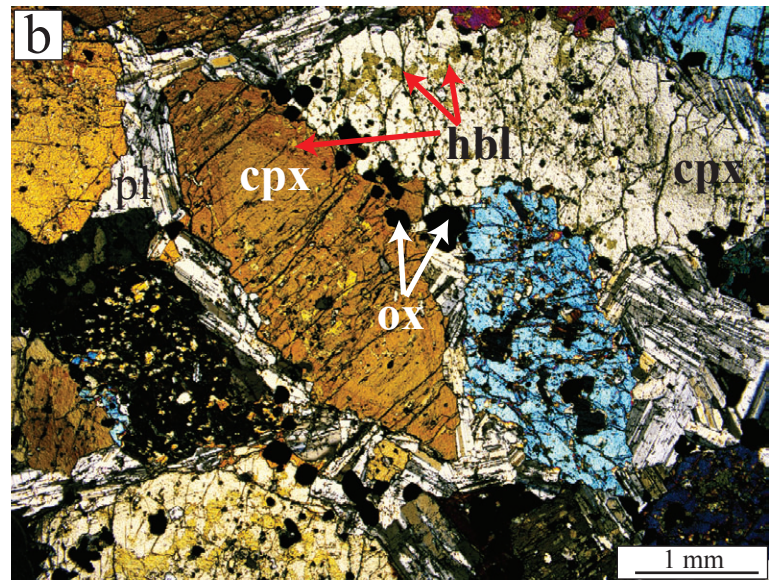
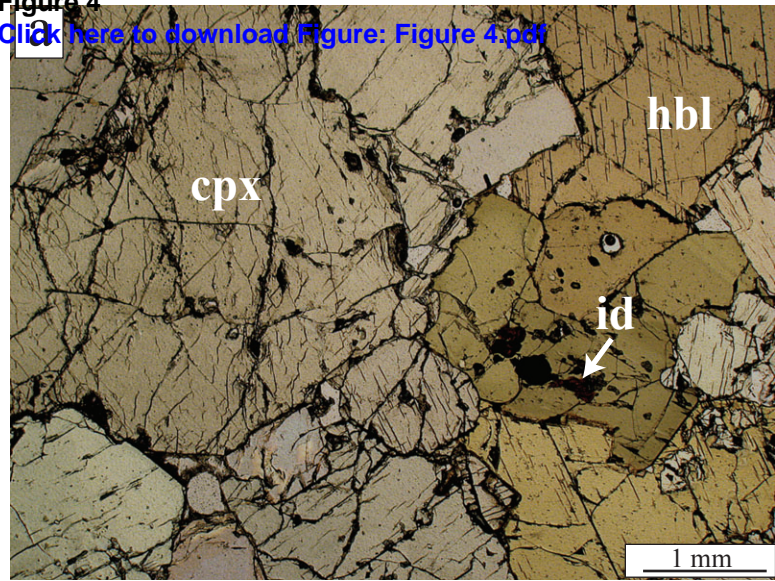


Figure 5

[Click here to download Figure: Figure 5.pdf](#)

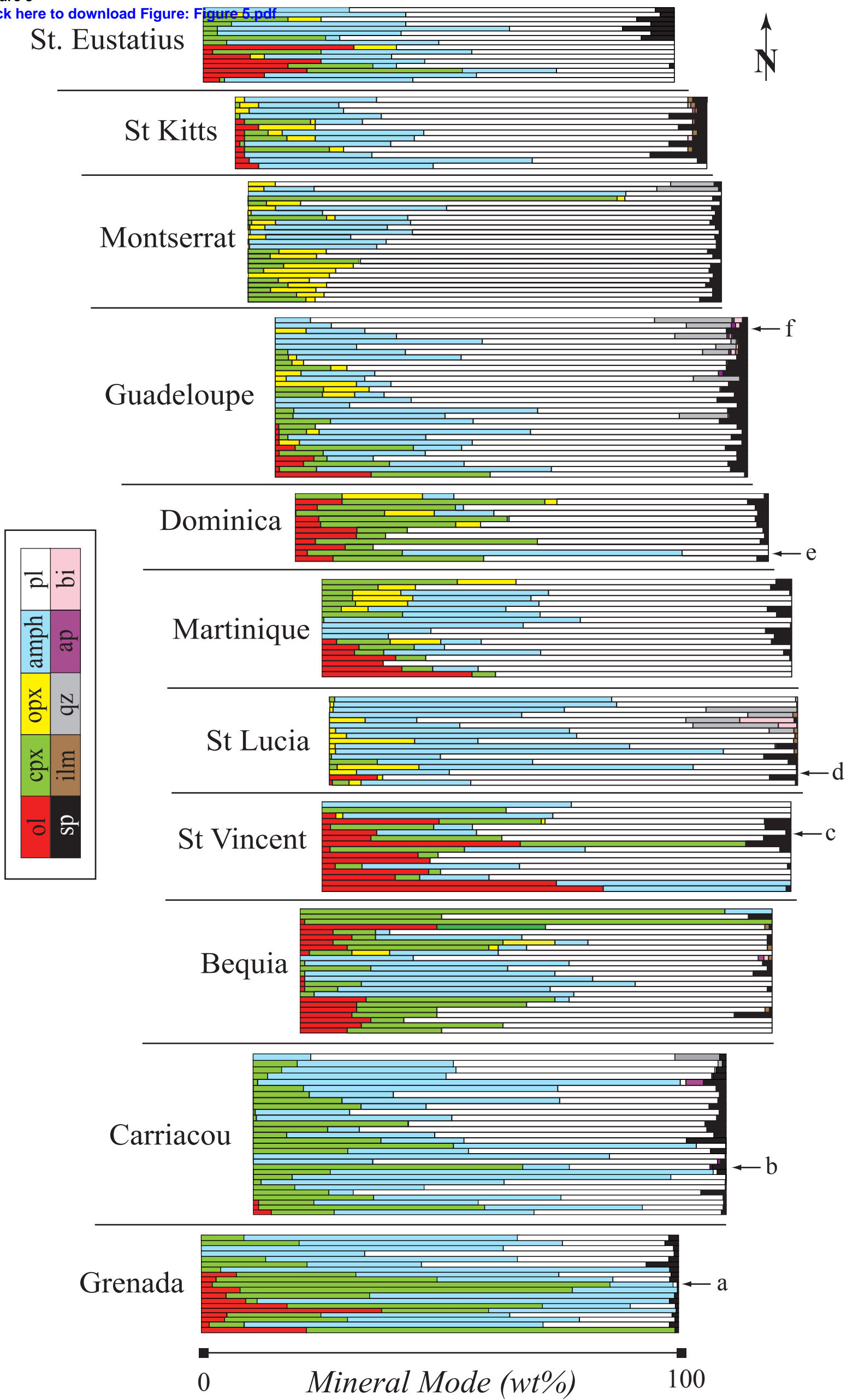


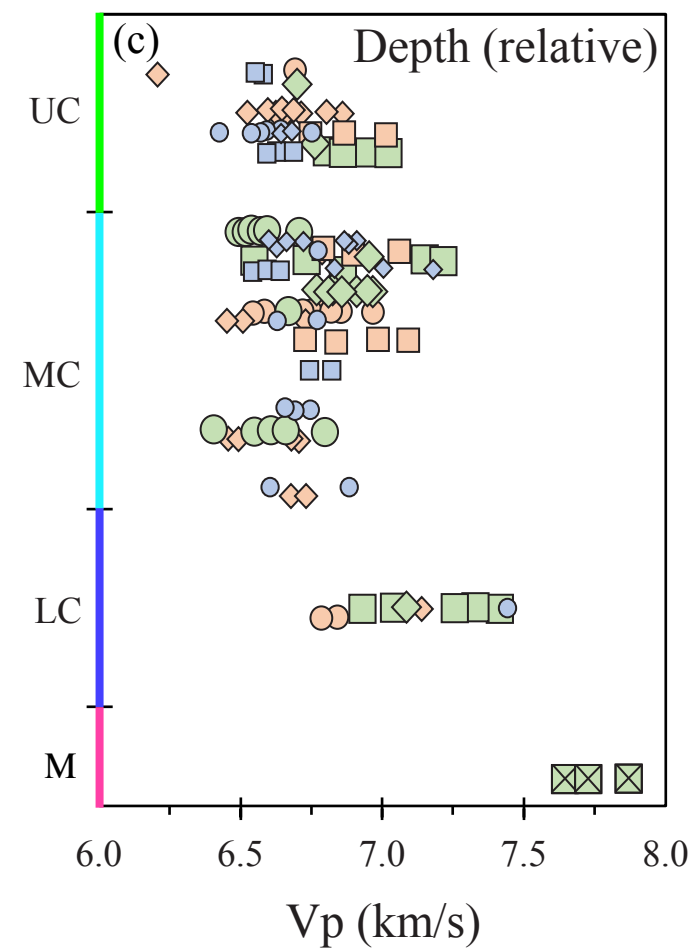
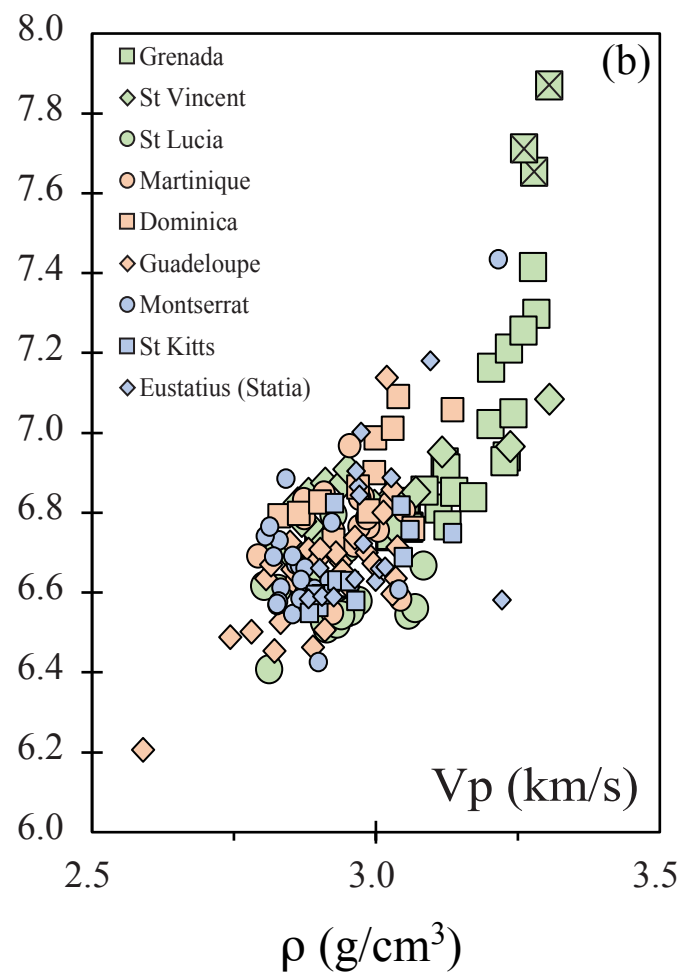
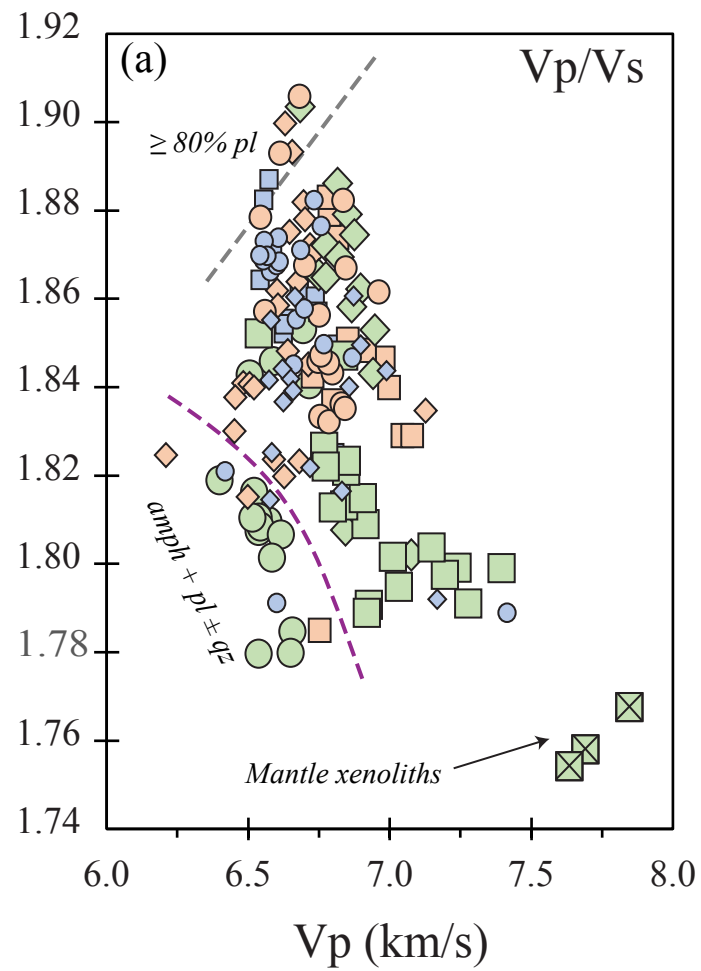
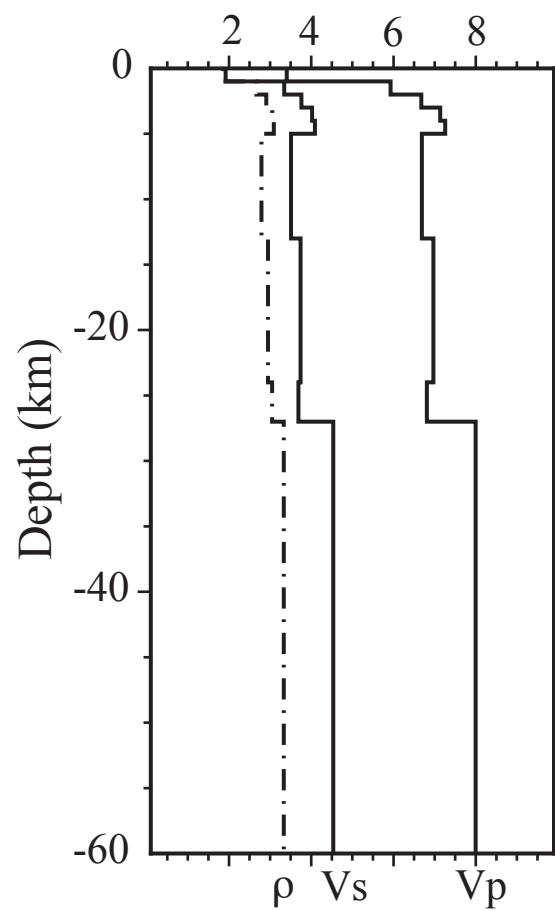
Figure 6[Click here to download Figure: Figure 6.pdf](#)

Figure 7

[Click here to download Figure: Figure 7.pdf](#)

(a) Martinique



(b) Grenada

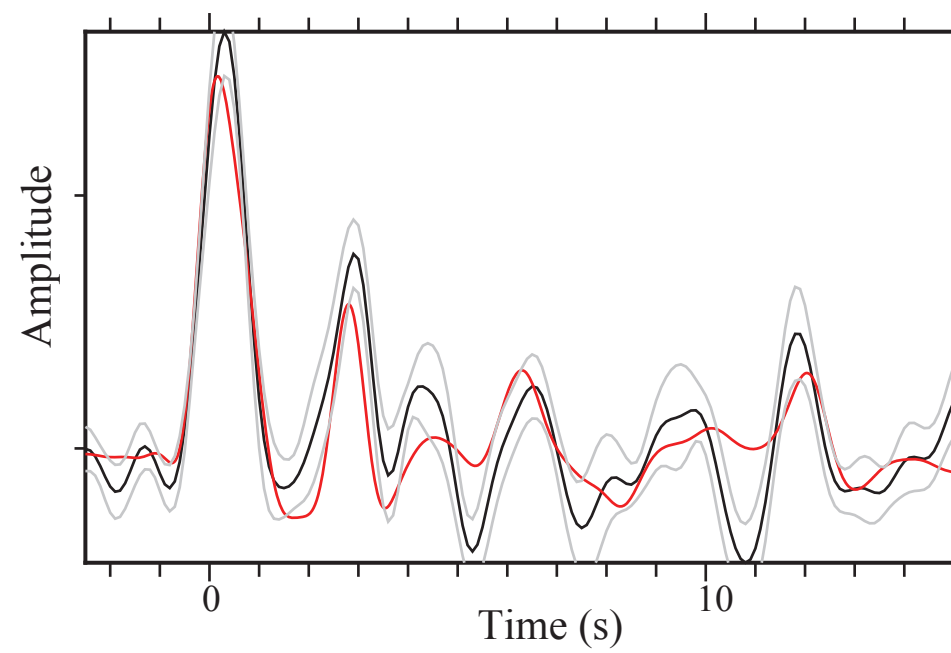
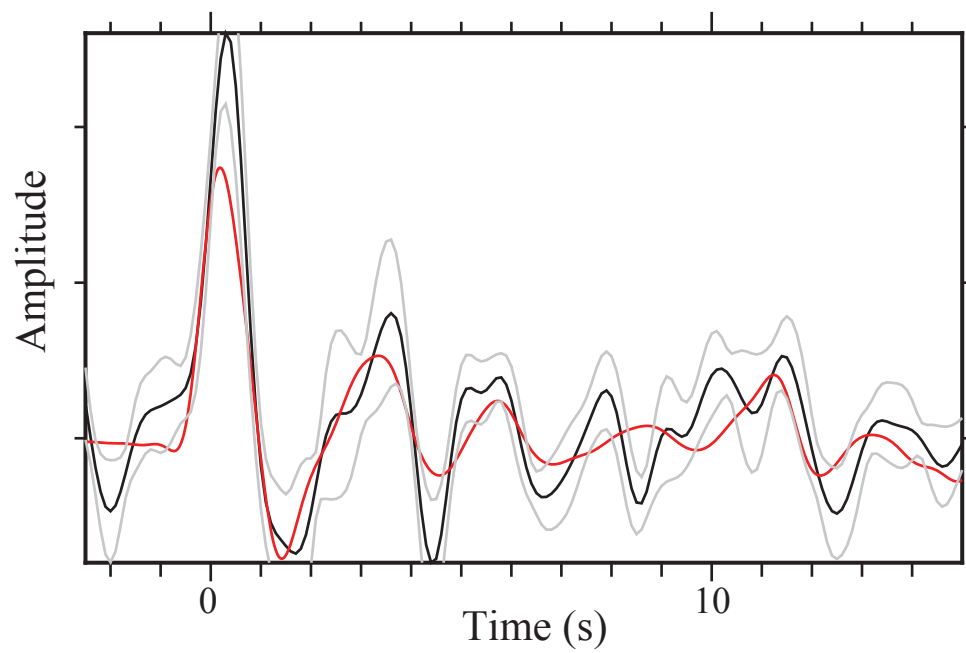
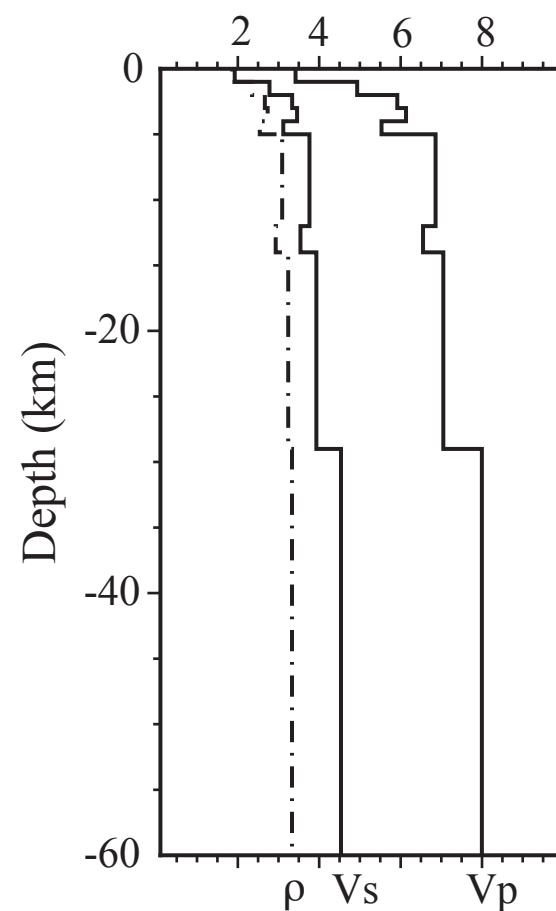


Figure 8

[Click here to download Figure: Figure 8.pdf](#)

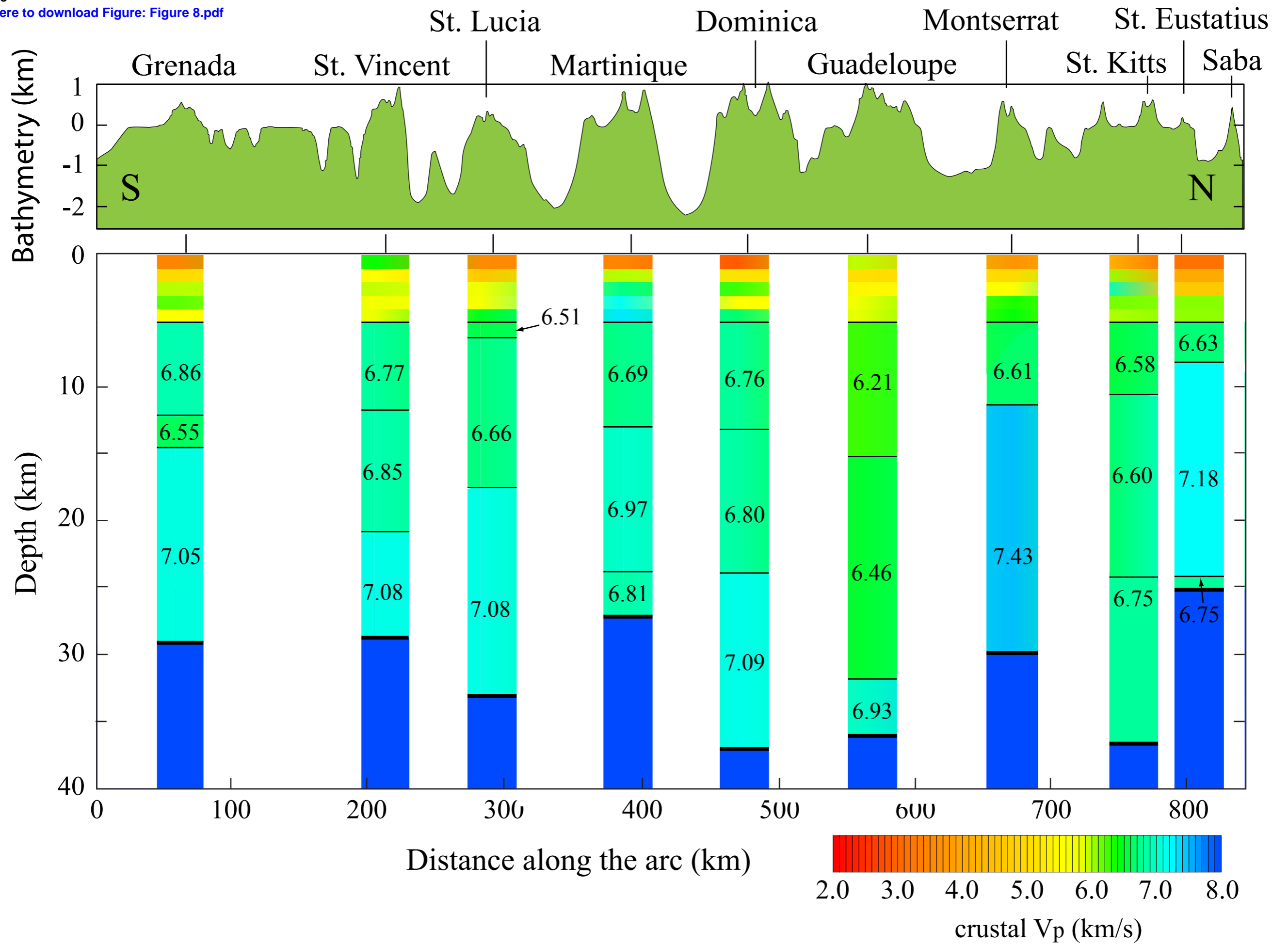


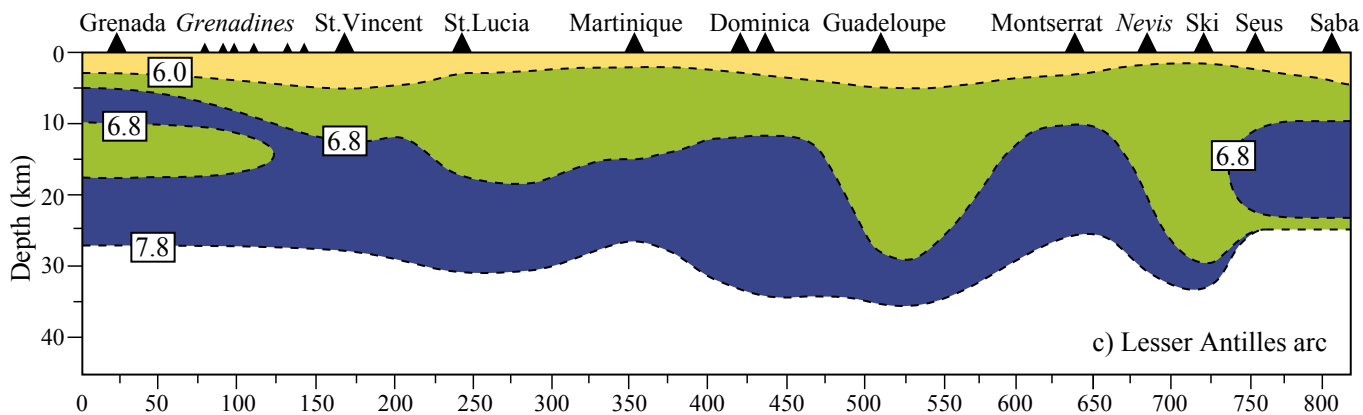
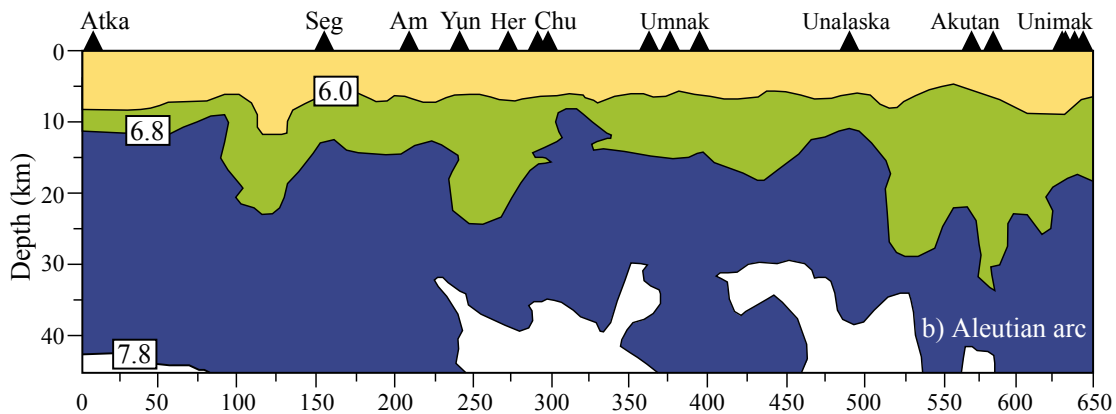
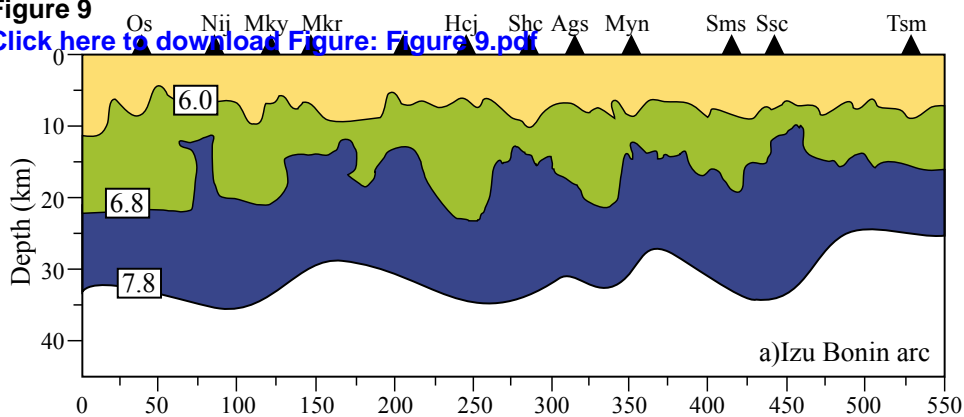
Figure 9[Click here to download Figure: Figure 9.pdf](#)

Figure 4 (high-resolution)

[Click here to download Figure \(high-resolution\): Figure 4.tif](#)

Table 1

[Click here to download Table: Table 1.docx](#)**Table 1.** The modeled velocity profiles and MCD and Moho depth.

	Layer (2)	v_p (km/s)	r (g/cm ³)	z^* (km)	Layer (3)	v_p (km/s)	r (g/cm ³)	z^* (km)	Layer (4)	v_p (km/s)	r (g/cm ³)	z^* (km)
<i>Grenada</i>	poikilitic-hornblende gabbro (GR4)	6.86	3.09	12	hornblende gabbro (GR42)	6.55	2.93	14	clinopyroxene hornblendite (GR17)	7.3	3.28	29
<i>St. Vincent</i>	hornblende troctolite (VS8)	6.77	2.88	12	plagioclase hornblendite (VS5)	6.85	3.07	21	olivine hornblende pyroxenite (VS20)	7.08	3.93	29
<i>St. Lucia</i>	hornblende leuco-norite (SL107)	6.51	2.91	6	hornblende norite (SL72)	6.66	2.89	17	olivine-hornblende pyroxenite (VS20)	7.08	3.93	33
<i>Martinique</i>	troctolite (MQ55)	6.69	2.79	13	olivine gabbro (MQ13)	6.97	2.95	24	hornblende gabbro norite (MQ12)	6.81	3.05	25
<i>Dominica</i>	olivine hornblende gabbro (D214)	6.76	3.07	13	olivine hornblende gabbro norite (D410)	6.80	2.99	23	olivine gabbro (D250c)	7.09	3.04	25
<i>Guadeloupe</i>	granodiorite (GD43)	6.21	2.59	15	diorite (GD39)	6.46	2.89	32	hornblendite (GR25)	6.93	3.23	36
<i>Montserrat</i>	–	-	-	-	plagioclase hornblendite (FB220)	6.61	3.04	11	plagioclase pyroxenite (300a)	7.43	3.22	30
<i>St. Kitts</i>	olivine norite (KS11)	2.96	6.58	10	olivine hornblende gabbro (KS22)	2.9	6.6	19	olivine hornblende gabbro (KS15)	6.75	3.14	37
<i>St. Eustatius</i>	hornblende gabbro norite (EU22)	6.63	2.96	8	olivine hornblende gabbro (EU77)	7.18	3.10	24	olivine hornblende gabbro (KS15)	6.75	3.14	25

 z^* - depth to the bottom of the layer

Supplementary Table S1

[Click here to download Supplementary material for online publication only: Supp.Table S1.xlsx](#)

Supplementary Table S2

[Click here to download Supplementary material for online publication only: Supp.Table S2.xlsx](#)

Supplementary RF modelling

[Click here to download Supplementary material for online publication only: Supplementary Material_RFmodelling.pdf](#)